# Contents

# 1 Models and Discretization

In this chapter, the mathematical description of the multi-scale model and its discretization is presented. We use the multi-scale chemo-electro-mechanical model that was introduced in literature [Röh12]; [Hei13]; [Hei15]; [Mor15]. Additional models known from literature are incorporated that were previously only simulated in isolation: The multidomain description for electrophysiology [Klo20], a model of neural stimulation [Cis08] and sensory organ models such as the muscle spindle model of Mileusnic et al. [Mil06b]. Similarly, models of Golgi tendon organs can be added [Mil06a].

Figure 1.1 shows an overview of the components of the implemented multi-scale model. A pool of motor neurons drives the stimulation of the muscular system in Fig. 1.1 (a). The axons of each motor neuron innervate the muscle fibers corresponding to the same MU and transmit rate-encoded stimulation signals.

In the muscle tissue, action potentials propagate starting at the neuromuscular junctions and subsequently reach the whole length of the muscle. In our multi-scale model, two different formulations are available to describe this phenomenon. The multidomain description (Fig. 1.1 (b1)) models the MUs from a homogenized 3D perspective. The description with muscle fibers (Fig. 1.1 (b2)) models action potential propagation explicitely with $n$ 1D muscle fibers.

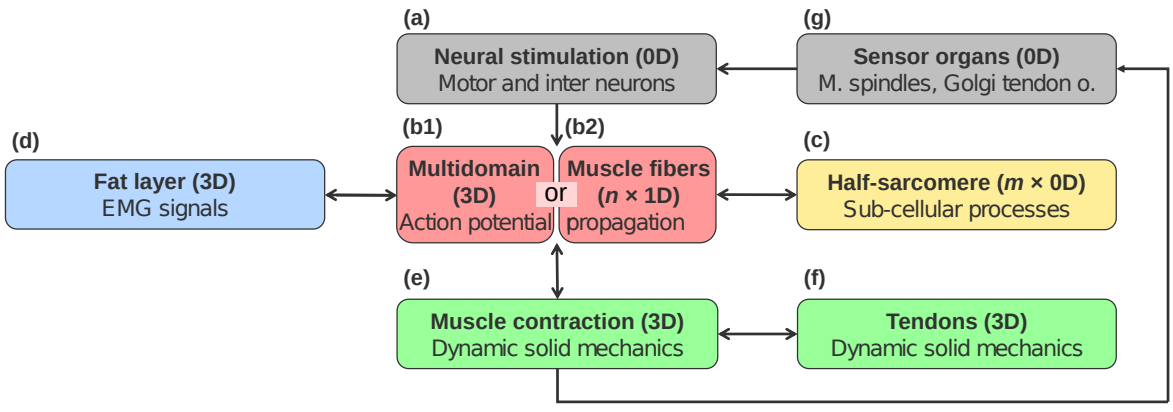


Figure 1.1: Interacting components of the multi-scale model.

Both of these descriptions of electrophysiology involve a subcellular model (Fig. 1.1 (c)). This model describes the ionic processes involving the fiber membranes and taking place within one half of a sarcomere as the smallest unit to generate muscle forces. A large number $m$ of instances of this model has to be computed.

In addition to the physiology of the muscle, a layer of body fat and skin on top of the muscle belly can be added to the model. This 3D fat layer (Fig. 1.1 (d)) is used to simulate EMG recordings on the skin surface. The model for the fat layer is unidirectionally coupled with the muscle fiber model (Fig. 1.1 (b2)) or bidirectionally coupled with the multidomain model (Fig. 1.1 (b1)). Using the multidomain model, it is, thus, possible to simulate external stimulation by electrodes on the skin, which is subject to research in neuroprosthetics.

The activated muscle generates force by subcellular proceses on a molecular scale. They are computed on the cellular level by the half-sarcomere model (c). On the macroscopic scale, stresses lead to strains and contraction of the muscle. This effect is described by the muscle contraction model on a 3D domain (Fig. 1.1 (e)). The description is coupled with the electrophysiology models (b1),(b2) by the geometry of the contracting muscle and fibers. It is coupled with the subcellular model by the generated active stresses of the half-sarcomere. Displacements and stresses can be computed for the muscle belly itself, but also for the connected body fat layer and for elastic tendons (Fig. 1.1 (f)). Depending on the research questions, the contraction model is either formulated quasi-static or fully dynamic taking into account inertia effects.

Sensory organs such as muscle spindles and Golgi tendon organs sense fiber stretch and contraction velocity (Fig. 1.1 (g)). They are connected with the motor neuron pool by layers of interneurons and modulate the stimulation in Fig. 1.1 (a).

In this chapter, Sec. 1.1 presents mathematical descriptions of all model components in the multi-scale framework and Sec. 1.3 addresses their discretization in time and space. An own section, Sec. 1.4, is dedicated to the discretization and solution of the mechanics model.

## 1.1 Model Equations

In the following, more details and mathematical descriptions are given for the outlined models. The section begins with the 0D half-sarcomere model in Sec. 1.1.1, followed by the bidomain and monodomain models in Sections 1.1.2 and 1.1.3, which constitute

the muscle fiber based model of electrophysiology. Section 1.1.4 continues with the multidomain model. Electric conduction in the body fat layer is described in Sec. 1.1.5. An overview of the continuum mechanics model used for muscle contraction is given in Sec. 1.2.

### 1.1.1 Subcellular Model

Propagation of electric stimuli along muscle fibers involves activation and deactivation of ion channels and ion pumps in the fiber membrane (the sarcolemma) and in the transverse tubules. Functioning of these processes on the subcellular scale have first been suggested in 1952 by Hodgkin and Huxley after their studies of the squid giant axons [Hod52a]; [Hod52b]. To date, their mathematical model still serves as the basis for electrophysiology models and some of their predictions, e.g., on gating currents that occur during opening of channels, were experimentally confirmed later.

The fiber membrane separates intra- and extracellular space and can be locally described by an electric circuit. The membrane voltage $V_m = \phi_i - \phi_e$ is the difference between the intra and extracellular potentials $\phi_i$ and $\phi_e$. The membrane stores charges $Q$, quantifiable by its electric capacitance $C_m$:

$$Q = C_m \cdot V_m. \tag{1.1}$$

A change in the transmembrane potential, e.g., induced by an action potential leads to a change in $Q$, which is accounted for by an electric current $I$ over the membrane. This can be formally obtained by the derivative of Eq. (1.1) with respect to time:

$$\frac{\mathrm{d}Q}{\mathrm{d}t} = C_m \cdot \frac{\mathrm{d}V_m}{\mathrm{d}t}. \tag{1.2}$$

The current $I = \mathrm{d}Q/\mathrm{d}t$ is realized by ions passing through the membrane. Significant ions in this process are sodium ($Na^+$) and potassium ions ($K^+$). Considering a particular point on the fiber, these ions diffuse through ion-specific channels in the membrane. The diffusion is driven by an interplay of the ion concentration gradient and the electric field that is caused by action potentials.

Without any electric field imposed by action potentials, the equilibrium state of the diffusion process for sodium and potassium ions is given by their Nernst potentials $E_{Na^+}$ and $E_{K^+}$. These voltage levels depend on logarithmic relations between extra- and intracellular concentrations scaled by constants describing the thermic energy and the number

of electrons. In thermodynamic equilibrium, the membrane voltage is equal to the Nernst potential $E_i$ of the involved ions $i$. At a higher membrane voltage $V_m$, the remainder $(V_m - E_i)$ is the part of the electric field that drives the ion fluxes and electric currents through the membrane. The currents depend on the conductivity $g_i$ of the membrane for ion $i$.

Apart from sodium and potassium ions, the diffusion of less frequent ions and ionic pumps can be lumped by a leakage current $I_L$ that is modeled by a channel with constant conductivity $\bar{g}_L$. With this, the total ionic membrane current $I_{\text{ion}}$ is formulated as

$$I_{\text{ion}}(V_m) = I_{\text{Na}^+} + I_{\text{K}^+} + I_L \tag{1.3a}$$

$$= g_{\text{Na}^+}(V_m - E_{\text{Na}^+}) + g_{\text{K}^+}(V_m - E_{\text{K}^+}) + \bar{g}_L(V_m - E_L). \tag{1.3b}$$

The conductivities $g_{\text{Na}^+}$ and $g_{\text{K}^+}$ for the sodium and potassium channels depend on the transmembrane voltage $V_m$ and its history.

In addition to the ionic current $I_{\text{ion}}$, an externally driven current $I_{\text{ext}}$ can be modeled that occurs as a result of neural stimulation at the neuromuscular junctions. Substituting the current $I = \mathrm{d}Q/\mathrm{d}t$ in Eq. (1.2), we get the following differential equation for the membrane voltage $V_m$:

$$C_m \cdot \frac{\mathrm{d}V_m}{\mathrm{d}t} = -I_{\text{ion}}(V_m) + \frac{I_{\text{ext}}}{A}. \tag{1.4}$$

The negative sign of the ionic current $I_{\text{ion}}$ is in accordance with the definition of the membrane voltage as $V_m = \phi_i - \phi_e$. The external current $I_{\text{ext}}$ is divided by the surface area $A$ of the stimulating electrode or neuromuscular junction, as the description considers an infinitesimal area on the membrane.

Hodgkin and Huxley suggested that ion channels can be activated and deactivated. This molecular process requires independent "gating" particles to move to a new position in order for a channel to be activated. For the potassium channel, four of these independent events have to occur, each modeled by a propability $n$. The resulting probability for the channel to open is, thus, $n^4$. For the sodium channel, three such events are assumed for activation and another one for the deactivation of the channel, described by the propabilities $m$ and $h$, respectively. The values of the probabilities change over time and modulate the conductivities of the ion channels:

$$g_{\text{Na}^+} = \bar{g}_{\text{Na}^+} \cdot m(t)^3 \cdot h(t), \qquad g_{\text{K}^+} = \bar{g}_{\text{K}^+} \cdot n(t)^4.$$

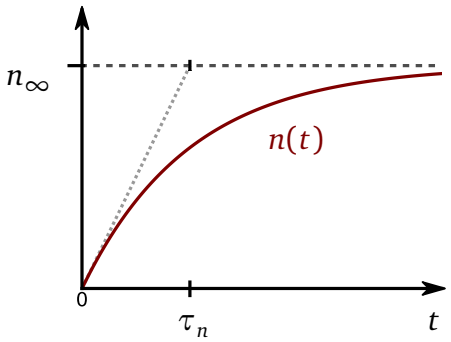


Figure 1.2: Subcellular model: Graph of the analytic solution (red) of the ordinary differential equation that is part of the activation model of ion channels for constant transmembrane voltage and initial condition $n(0) = 0$, given in Eq. (1.5). The variables $n_\infty$ and $\tau_n$ can be interpreted as the equilibrium value and a characteristic time scale, respectively.

Here, $\bar{g}_{\mathrm{Na}^+}$ and $\bar{g}_{\mathrm{K}^+}$ are channel specific constants. The gating variables $n, m$ and $h$ can be interpreted as probabilities for the events to occur or as the amount of occured events related to all available gating particles. The evolution of the activation probability $n$ is modeled by the following ordinary differential equation (ODE):

$$\frac{\mathrm{d}n}{\mathrm{d}t} = \alpha_n(V_m) \cdot (1-n) + \beta_n(V_m) \cdot n,$$

analogously for $h$ and $n$. The transition rates between activation probability $n$ and deactivation probability $(1-n)$ are nonlinearly dependent on the membrane voltage $V_m$.

For a constant $V_m$, this ODE has an analytical solution

$$n(t) = n_\infty\big(1 - \exp(1 - \frac{1}{\tau_n}\, t)\big), \tag{1.5}$$

which for $t \to \infty$ converges to the equilibrium value $n_\infty := \alpha_n\, \tau_n$ as shown in Fig. 1.2. The time constant $\tau_n := 1/(\alpha_n + \beta_n)$ indicates how fast the solution approaches the equilibrium, e.g., when starting from $n(0) = 0$, half of the value of the equilibrium is reached after $t_{1/2} = \log(2)\, \tau_n$. The smaller $\tau_n$, the stiffer is the ODE, which needs to be considered in the choice of a suitable numerical solution scheme.

Because the transmembrane voltage $V_m$ changes over time, the ODEs for $n, m$ and $h$ have to be solved numerically. Then, the dependent ionic current $I_{\mathrm{ion}}$ can be calculated. Thus, the model is a system of differential-algebraic equations (DAE).

The internal states in this model can be combined into a state vector $\mathbf{y} = (n, m, h)^\top$. The

combined right hand side for all states is formulated as a vector-valued function $G(V_m, \mathbf{y})$. In summary, the system of DAEs for the subcellular model on a subcellular domain $\Omega_s$ can be written in the following form:

$$\frac{\partial \mathbf{y}}{\partial t} = G(V_m, \mathbf{y}), \qquad I_{\text{ion}} = I_{\text{ion}}(V_m, \mathbf{y}) \quad \text{on } \Omega_s. \tag{1.6}$$

For an exemplary solution that shows how the membrane potential changes over time, see **??**.

The system of equations in Eq. (1.6) together with Eq. (1.4) describe the subcellular processes on a single point $\Omega_s \subset \Omega_f$ on a muscle fiber $\Omega_f$. It does not model the interaction between neighboring points that leads to propagation of action potentials. To account for action potential propagation, ionic currents $I_{\text{ion}}$ on multiple points are coupled within the multidomain or fiber models that are formulated in the multi-scale framework. This is described in the following sections, Sections 1.1.2 to 1.1.4. Using these models, the system of ODEs in Eq. (1.6) has to be solved for multiple subcellular points $\Omega_s^i$ in the muscle domain.

After Hodgkin and Huxley proposed this model in 1952, more detailed models were formulated that take into account more ion channels, ion pumps and more advanced biochemical processes within the cell. One particular model is the one proposed by Shorten et al. [Sho07], which adds the full pathway from activation to excitation-contraction coupling in the sarcomere. It has a state vector of $\mathbf{y} \in \mathbb{R}^{56}$ and is used to compute active stresses for simulations of muscle contraction. It can also be written in the form given in Eq. (1.6). Apart from $I_{\text{ion}}$, another value $\gamma = H(\mathbf{y}, \dot{\lambda}_f)$ is computed by an additional equation from the vector of states $\mathbf{y}$ and the fiber contraction velocity $\dot{\lambda}_f$, which is given to the model as a parameter. The value $\gamma$ is a lumped activation parameter in the range $\gamma \in [0, 1]$ that describes the amount of active stress generated in the sarcomere and can be linked to the continuum mechanics model of muscle contraction.

### 1.1.2 Bidomain Model

A description of electrophysiology on a general 3D muscle tissue is given by the bidomain model formulated by [Tun78]; [Pes79]. The bidomain model considers the intra (index $i$) and extracellular spaces (index $e$) in a homogenized setting, such that the two domains coexist at every spatial point $\mathbf{x} \in \Omega \subset \mathbb{R}^3$. Similar to the setting of the subcellular model, the two domains in the bidomain model have locally varying electric potential fields

$\phi_i$ and $\phi_e$ that yield a locally varying transmembrane voltage $V_m = \phi_i - \phi_e$. Electric conduction within the two domains is governed by conductivity tensors $\boldsymbol{\sigma}_i$ and $\boldsymbol{\sigma}_e$.

Assuming static conditions, a spatially varying electric potential $\phi$ induces the electric field $E = -\text{grad}\,\phi$. According to Ohm's law, the resulting current density $j$ is given by

$$j = \boldsymbol{\sigma}\, E = -\boldsymbol{\sigma}\,\text{grad}\,\phi \quad \text{in } \Omega. \tag{1.7}$$

This holds for both intra and extracellular domain, yielding expressions for $j_i$ and $j_e$.

The intracellular and the extracellular domain are electrochemically coupled. Thus, one assumption is that currents are preserved and a change in current density on one domain corresponds to the opposite change in current density in the other domain. This is expressed by the divergence of the current densities, which in one domain equals to the negated value in the other domain:

$$\text{div}\,(j_i) = -\text{div}\,(j_e) \quad \text{in } \Omega. \tag{1.8}$$

This change in current density directly corresponds to a current flow over the membrane:

$$\text{div}\,(j_i) = A_m\, I_m \quad \text{in } \Omega.$$

Here, the factor $A_m$ describes the membrane area to domain volume relationship. It is needed to convert the units between current per volume and current per area. The membrane current $I_m$ is given by the subcellular model of Hodgkin and Huxley in Eq. (1.4). Neglecting the external current $I_{\text{ext}}$ in Eq. (1.4) and using the formulation of the intracellular current density $j_i$ in Eq. (1.7), we get:

$$\text{div}\big(\boldsymbol{\sigma}_i\,\text{grad}\,(\phi_i)\big) = A_m\Big(C_m\,\frac{\partial V_m}{\partial t} + I_{\text{ion}}(V_m)\Big) \quad \text{in } \Omega.$$

The ionic current $I_{\text{ion}}$ can be computed by Eq. (1.3b). By plugging Eq. (1.7) also into Eq. (1.8) and rewriting the equations in terms of the extracellular potential $\phi_e$ and the transmembrane voltage $V_m = \phi_i - \phi_e$, we get the bidomain equations:

$$\text{div}\big((\boldsymbol{\sigma}_i + \boldsymbol{\sigma}_e)\,\text{grad}\,(\phi_e)\big) + \text{div}\,(\boldsymbol{\sigma}_i\,\text{grad}\,(V_m)\big) = 0, \tag{1.9a}$$

$$\text{div}\big(\boldsymbol{\sigma}_i\,\text{grad}\,(V_m)\big) + \text{div}\,(\boldsymbol{\sigma}_i\,\text{grad}\,(\phi_e)\big) = A_m\Big(C_m\,\frac{\partial V_m}{\partial t} + I_{\text{ion}}(V_m)\Big). \tag{1.9b}$$

With appropriate boundary conditions, these equations are often used to model cardiac electrophysiology. They also serve as a basis for the fiber models in our multi-scale setting, which will be described in the next section.

### 1.1.3 Monodomain Model

One approach to modeling skeletal muscle electrophysiology is to explicitly resolve muscle fibers and compute propagating action potentials on these spatial domains. Propagation of action potentials can be described by the monodomain equation, which is a specialization of the bidomain equations for a one-dimensional intracellular space.

We assume a muscle domain $\Omega_M \subset \mathbb{R}^3$ with a number of embedded 1D manifolds $\Omega_f^j \subset \mathbb{R}^3$ for $j = 1, \dots, n$ that represent muscle fibers. The domain $\Omega_M$ represents the extracellular space and each fiber domain $\Omega_f^j$ represents a separate intracellular space. It is further assumed that electric conduction in the extracellular space is directed equally to the embedded fibers. This can be stated as

$$\boldsymbol{\sigma}_i = k \cdot \boldsymbol{\sigma}_e. \tag{1.10}$$

The intracellular conductivity tensor $\boldsymbol{\sigma}_i$ (here prolonged from the scalar value $\sigma_i$ on a fiber with tangent $\mathbf{a} \in \mathbb{R}^3$ to the 3D domain by $\boldsymbol{\sigma}_i = \sigma_i \, \mathbf{a} \otimes \mathbf{a}$) and the extracellular conductivity $\boldsymbol{\sigma}_e$ are multiples of each other with a scaling factor $k \in \mathbb{R}$.

Plugging Eq. (1.10) into the first bidomain equation, Eq. (1.9a), and restricting the domain to a 1D fiber $\Omega_f^j$ allows to combine the terms related to $\phi_e$:

$$\operatorname{div}\big(\sigma_i \operatorname{grad}(\phi_e)\big) = -\frac{k}{k+1} \operatorname{div}\big(\sigma_i \operatorname{grad}(V_m)\big) \quad \text{on } \Omega_f^j.$$

Using the second bidomain equation, Eq. (1.9b), we get the expression

$$\operatorname{div}\big(\sigma_{\text{eff}} \operatorname{grad}(V_m)\big) = A_m\Big(C_m \frac{\partial V_m}{\partial t} + I_{\text{ion}}(V_m, \mathbf{y})\Big) \quad \text{on } \Omega_f^j.$$

The effective conductivity $\sigma_{\text{eff}}$ combines the intra and extracellular conductivities, $\sigma_i$ and $\sigma_e$, analogous to a parallel circuit:

$$\sigma_{\text{eff}} := \sigma_i \parallel \sigma_e = \frac{\sigma_i \, \sigma_e}{\sigma_i + \sigma_e}.$$

Rearranging the terms yields the classical form of the monodomain equation:

$$\frac{\partial V_m}{\partial t} = \frac{1}{A_m C_m}\left(\sigma_{\text{eff}} \frac{\partial^2 V_m}{\partial x^2} - A_m I_{\text{ion}}(V_m, \mathbf{y})\right) \qquad \text{for } x \in \Omega_f^j. \tag{1.11}$$

The multi-scale framework uses multiple instances of the monodomain equation Eq. (1.11) together with the first bidomain equation Eq. (1.9a) to model electrophysiology in the fibers and the extracellular domain [Mor15]. In addition to the fiber domains $\Omega_f^j$, two instances of the muscle domain $\Omega_M$ are needed for the bidomain equation, one for the intracellular and one for the extracellular space. The transmembrane potential $V_m$ is unidirectionally coupled from the fiber meshes to the intracellular space of the first bidomain equation. The extracellular potential $\phi_e$ corresponds to the signals that are measured during intramuscular EMG recording.

Within the multi-scale framework, it is also possible to couple a model for electric conduction in an additional layer of body fat tissue. This is subsequently described in Sec. 1.1.5. Then, electric current fluxes between the muscle and body fat domains have to be modeled.

If no such additions should be made to the model, the following Neumann boundary conditions are used to close the description:

$$\frac{\partial V_m}{\partial x} = 0 \qquad \text{on } \partial\Omega_f^j, \tag{1.12a}$$

$$\left(\boldsymbol{\sigma}_i \operatorname{grad}(V_m)\right) \cdot \mathbf{n}_m = -\left(\boldsymbol{\sigma}_i \operatorname{grad}(\phi_e)\right) \cdot \mathbf{n}_m \qquad \text{on } \partial\Omega_M, \tag{1.12b}$$

$$\left(\boldsymbol{\sigma}_e \operatorname{grad}(\phi_e)\right) \cdot \mathbf{n}_m = 0 \qquad \text{on } \partial\Omega_M, \tag{1.12c}$$

with the outward normal vector $\mathbf{n}_m$. Equation (1.12a) defines homogeneous Neumann boundary conditions for the monodomain equation Eq. (1.11) at the two ends of each 1D muscle fiber domain. The boundary conditions on $\partial\Omega_M$ are related to the bidomain equations given in Eqs. (1.9a) and (1.9b). Equation (1.12b) is equivalent to a homogeneous Neumann boundary condition on the intracellular current density $j_i$ (cf. Eq. (1.7)) and is expressed in terms of the transmembrane voltage $V_m$ and the extracellular potential $\phi_e$. Another homogeneous Neumann boundary condition on $\phi_e$ as given by Eq. (1.12c) is required.

### 1.1.4 Multidomain Model

The multidomain model is an alternative approach to the description based on the monodomain and bidomain equations described in Sections 1.1.2 and 1.1.3. It was proposed in [Klo20] and describes the same physics. However, the muscle fibers are homogenized and all equations are formulated using a single 3D muscle domain $\Omega_M$.

The multidomain equations generalize the two bidomain equations and allow to take into account multiple MUs by defining a separate intracellular space for each MU. Thus, at every spatial point $\mathbf{x} \in \Omega_M$ one extracellular and $N_{\mathrm{MU}}$ intracellular domains or compartments coexist, where $N_{\mathrm{MU}}$ is the number of MUs. As before, the extracellular domain has the electric potential $\phi_e$ and conductivity tensor $\boldsymbol{\sigma}_e$. For each compartment $k = 1, \dots, N_{\mathrm{MU}}$, a separate electric potential $\phi_i^k$, transmembrane voltage $V_m^k = \phi_i^k - \phi_e$, conductivity tensor $\boldsymbol{\sigma}_i^k$, surface to volume ratio of the membrane $A_m^k$ and membrane capacitance $C_m^k$ are defined.

Analogous to the fibers of a MU that exhibit different densities at different locations in the muscle, each compartment occupies different locations within the domain to a different extent. This is described by the relative occupancy factor $f_r^k : \Omega_M \to [0,1]$ for MU $k$. The factors have different values in the domain according to the presence of the MU at the respective location. At every point, their sum is one, $\sum_{k=1}^{N_{\mathrm{MU}}} f_r^k = 1$, if all MUs should be considered or less than one if the effect of remainder MUs that will not be activated in the simulation scenario is neglected.

The first multidomain equation is similar to the first bidomain equation Eq. (1.9a) and balances the current flow between the extracellular space and the weighted sum of all intracellular spaces:

$$\operatorname{div}\left(\boldsymbol{\sigma}_e \operatorname{grad}(\phi_e)\right) + \sum_{k=1}^{N_{\mathrm{MU}}} f_r^k \operatorname{div}\left(\boldsymbol{\sigma}_i^k \operatorname{grad}(V_m^k + \phi_e)\right) = 0. \tag{1.13}$$

By defining a total intracellular conductivity tensor $\boldsymbol{\sigma}_i = \sum_{k=1}^{N_{\mathrm{MU}}} f_r^k \boldsymbol{\sigma}_i^k$, Eq. (1.13) can be restated as

$$\operatorname{div}\left((\boldsymbol{\sigma}_e + \boldsymbol{\sigma}_i) \operatorname{grad}(\phi_e)\right) + \sum_{k=1}^{N_{\mathrm{MU}}} f_r^k \operatorname{div}\left(\boldsymbol{\sigma}_i^k \operatorname{grad}(V_m^k)\right) = 0. \tag{1.14}$$

The second multidomain equation equals the second bidomain equation Eq. (1.9b). It

describes the current over the membrane and holds for every compartment:

$$\operatorname{div}\left(\boldsymbol{\sigma}_i^k \operatorname{grad}\left(V_m^k + \phi_e\right)\right) = A_m^k \left(C_m^k \frac{\partial V_m^k}{\partial t} + I_{\text{ion}}(V_m^k)\right) \qquad \forall k \in \{1, \ldots, N_{\text{MU}}\}.$$

It is convenient to rearrange it for $\partial V_m^k / \partial t$:

$$\frac{\partial V_m^k}{\partial t} = \frac{1}{A_m^k C_m^k} \left(\operatorname{div}\left(\boldsymbol{\sigma}_i^k \operatorname{grad}\left(V_m^k + \phi_e\right)\right) - A_m^k I_{\text{ion}}(V_m^k)\right) \quad \forall k \in \{1, \ldots, N_{\text{MU}}\}. \tag{1.15}$$

The current $I_{\text{ion}}$ over the membrane is again computed by the subcellular model given by Eq. (1.3b).

The resulting system of Eqs. (1.14) and (1.15) constitutes the first and second multidomain equations and can be used to compute muscle electrophysiology. The boundary conditions are defined analogously to Eqs. (1.12b) and (1.12c):

$$\left(\boldsymbol{\sigma}_i^k \operatorname{grad}\left(V_m^k\right)\right) \cdot \mathbf{n}_m = -\left(\boldsymbol{\sigma}_i^k \operatorname{grad}\left(\phi_e\right)\right) \cdot \mathbf{n}_m \qquad \text{on } \partial\Omega_M \qquad \forall k \in \{1, \ldots, N_{\text{MU}}\}, \tag{1.16a}$$

$$\left(\boldsymbol{\sigma}_e \operatorname{grad}\left(\phi_e\right)\right) \cdot \mathbf{n}_m = 0, \qquad \text{on } \partial\Omega_M \tag{1.16b}$$

where $\mathbf{n}_m$ is the outward normal vector on $\partial\Omega_M$.

### 1.1.5 Electric Conduction in the Body Domain

Surface EMG signals are the result of electric conduction in the electrically active muscle tissue as well as in surrounding inactive tissue such as adipose tissue and skin or connective tissue such as tendons and ligaments. This surrounding tissue is summarized by the body domain $\Omega_B$, which partly shares its boundary with the muscle domain $\Omega_M$.

Figure 1.3 visualizes these domains and defines their names: The domains $\Omega_M$ and $\Omega_B$ have outward normals $\mathbf{n}_m$ and $\mathbf{n}_b$, the outer boundary is composed of $\Gamma_B^{\text{out}}$ and $\Gamma_M^{\text{out}}$ and the variables $\phi_e, V_m$ and $\phi_b$ are defined as shown within the domains $\Omega_M$ and $\Omega_B$.

The work of [Mor15] proposes an isotropic conductivity $\boldsymbol{\sigma}_b$ and a harmonic electric potential $\phi_b$ in the body domain $\Omega_B$:

$$\operatorname{div}\left(\boldsymbol{\sigma}_b \operatorname{grad}\left(\phi_b\right)\right) = 0 \qquad \text{on } \Omega_B. \tag{1.17}$$

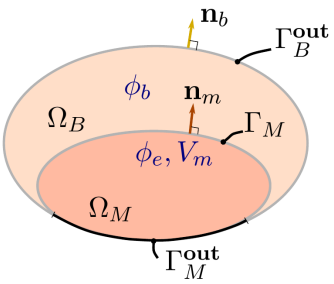


Figure 1.3: Computational domains for the simulation of surface EMG. The body domain $\Omega_B$ and the muscle domain $\Omega_M$ share a part of their boundary, $\Gamma_M$, which has a normal vector $\mathbf{n}_m$. The outer boundary is composed of $\Gamma_B^{\text{out}}$ and $\Gamma_M^{\text{out}}$ and has the outward normal vector $\mathbf{n}_b$.

The electric potentials $\phi_e$ and $\phi_b$ of the neighboring domains $\Omega_M$ and $\Omega_B$ as well as the current densities are continuous on the shared boundary $\Gamma_M$. This is described by the following two coupling conditions:

$$\phi_e = \phi_b \qquad \text{on } \Gamma_M, \tag{1.18a}$$

$$\big(\boldsymbol{\sigma}_e \operatorname{grad}(\phi_e)\big) \cdot \mathbf{n}_m = \big(\boldsymbol{\sigma}_b \operatorname{grad}(\phi_b)\big) \cdot \mathbf{n}_m \qquad \text{on } \Gamma_M. \tag{1.18b}$$

On the outer boundary $\Gamma_B^{\text{out}}$, homogeneous Neumann boundary conditions are assumed:

$$\big(\boldsymbol{\sigma}_b \operatorname{grad}(\phi_b)\big) \cdot \mathbf{n}_b = 0 \qquad \text{on } \Gamma_B^{\text{out}}. \tag{1.19}$$

The description of the body domain has to be combined either with the fiber based description in Sec. 1.1.3 or the multi-domain description in Sec. 1.1.4. In the literature, this combination was mathematically described for the fiber based model in [Mor15] and for the multidomain model in [Klo20]. Correspondingly, additional boundary conditions either given by Eq. (1.12) or Eq. (1.16) are assumed: For the fiber based description, which uses the bidomain equation for volume conduction, the boundary conditions are:

$$\big(\boldsymbol{\sigma}_i \operatorname{grad}(V_m)\big) \cdot \mathbf{n}_m = -\big(\boldsymbol{\sigma}_i \operatorname{grad}(\phi_e)\big) \cdot \mathbf{n}_m \qquad \text{on } \partial\Omega_M = \Gamma_M \cup \Gamma_M^{\text{out}}, \tag{1.20a}$$

$$\big(\boldsymbol{\sigma}_e \operatorname{grad}(\phi_e)\big) \cdot \mathbf{n}_m = 0 \qquad \text{on } \partial\Gamma_M^{\text{out}}. \tag{1.20b}$$

For the multidomain description with fat layer, the boundary conditions are:

$$\left(\boldsymbol{\sigma}_i^k \operatorname{grad}(V_m^k)\right) \cdot \mathbf{n}_m = -\left(\boldsymbol{\sigma}_i^k \operatorname{grad}(\phi_e)\right) \cdot \mathbf{n}_m \qquad \text{on } \partial\Omega_M = \Gamma_M \cup \Gamma_M^{\text{out}}, \tag{1.21a}$$

$$\left(\boldsymbol{\sigma}_e \operatorname{grad}(\phi_e)\right) \cdot \mathbf{n}_m = 0 \qquad \text{on } \partial\Gamma_M^{\text{out}}. \tag{1.21b}$$

The first condition in Eq. (1.21a) is enforced for all compartments $k = 1, \ldots, N_{\text{MU}}$.

## 1.2 Model of Muscle Contraction

Muscle contraction is described on the organ level by a solid mechanics model. The goal is to describe the deformation of the tissue caused by the internal forces that are generated by sarcomeres and as a response to outer constraints such as applied forces, the attachment to tendons and inertia effects.

Different modeling approaches exist to describe the mechanical muscle behavior. Dynamic *finite elasticity* methods for large strains exist that use hyperelastic materials, both compressible and incompressible. Further, *linear elasticity* descriptions with linearizations at various levels are used in appropriate applications where small strains can be assumed. The whole range from simplifying linearized models to accurate nonlinear approaches can be found in the literature, sometimes with varying conventions and symbols. In this section, we introduce consistent notation and formulate the model equations for both approaches. The discretization and solution is discussed later in Sec. 1.4.

The derivation largely follows the book of Holzapfel [Hol00] and the discretization follows the work of Zienkiewicz, Taylor et al. [Zie77]; [Zie05]. Further details can be found also in the book of Marsden and Hughes [Mar94].

### 1.2.1 Geometric Description

We begin with the geometric description of the material body and define the basic quantities that are subsequently used to describe the physics. We consider the 3D muscle domain $\Omega_0 = \Omega_M \subset \mathbb{R}^3$ in reference configuration at time $t = 0$ that deforms into a current configuration $\Omega_t$ at time $t$. The material points are given by $\mathbf{X} \in \Omega_0$. The corresponding points $\mathbf{x} \in \Omega_t$ in the current configuration are defined by the function $\mathbf{x} = \varphi_t(\mathbf{X})$.

In the following, capital letters refer to quantities in material or Lagrangian description, i.e., defined in the reference configuration and small letters refer to quantities in spatial or Eulerian description, i.e., defined in the current configuration.

The relation of point coordinates in the current configuration with respect to the reference configuration can also be described by the displacements field $\mathbf{U}$:

$$\mathbf{x}(\mathbf{X}) = \mathbf{X} + \mathbf{U}(\mathbf{X}).$$

The symbol $\mathbf{u}$ with $\mathbf{u}(\mathbf{x}(\mathbf{X})) = \mathbf{U}(\mathbf{X})$ denotes the displacements formulated in current configuration. The current velocity $\mathbf{v}$ is the time derivative of the displacements, $\mathbf{v} := \dot{\mathbf{u}}$.

The deformation gradient $\mathbf{F}$ is the second order tensor that is obtained by differentiating the function $\varphi_t$. It is given using the unit vectors $\mathbf{e}_i$ and components $F_{aA}$:

$$\mathbf{F} = F_{aA}\,\mathbf{e}_a \otimes \mathbf{e}_A, \qquad F_{aA} = \frac{\partial x_a}{\partial X_A}.$$

Capital and small indices refer to reference and current configuration, respectively. The deformation gradient can also be expressed using the displacement field $\mathbf{U}$:

$$\mathbf{F} = \mathbf{I} + \nabla \mathbf{U}. \tag{1.22}$$

Here and in the following, the gradient symbol $\nabla$ refers to differentiation with respect to material coordinates $\mathbf{X}$. We assume cartesian coordinates.

The determinant of the deformation gradient is $J := \det \mathbf{F} > 0$. It is positive for any physically valid transformation. The deformation gradient is used to map geometric quantities from the reference to the current configuration:

$$\mathbf{t} = \mathbf{F}\,\mathbf{T}, \qquad \text{(tangent map)} \tag{1.23a}$$

$$\mathbf{a} = \operatorname{cof}(\mathbf{F})\,\mathbf{A}, \qquad \text{(normal map)} \tag{1.23b}$$

$$v = J\,V. \qquad \text{(volume map)} \tag{1.23c}$$

As given in Eq. (1.23a) and visualized in Fig. 1.4, the tensor $\mathbf{F}$ maps material tangents $\mathbf{T}$ in $\Omega_0$ to the corresponding spatial line elements $\mathbf{t}$ in $\Omega_t$. Accordingly, the spatial stretch at a point $\mathbf{x} \in \Omega_t$ in a certain direction is given by $\lambda = \sqrt{\boldsymbol{\lambda}^\top \boldsymbol{\lambda}}$ with $\boldsymbol{\lambda} = \mathbf{F}\,\mathbf{M}$, where $\mathbf{M}$ is a material line element with unit length pointing in the respective Lagrangian direction.

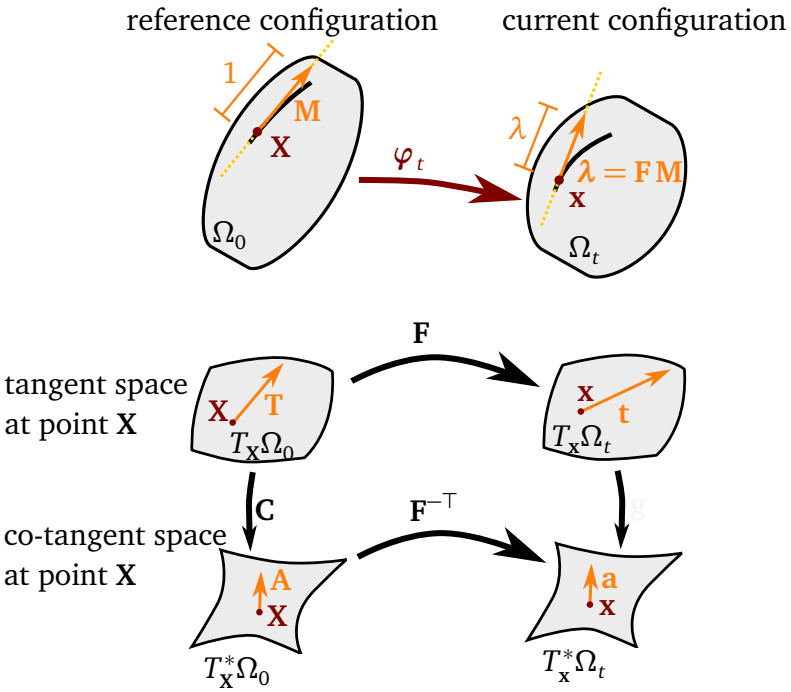


Figure 1.4: Vector spaces and variables used in the geometric description of the solid mechanics model. The left side shows the reference configuration with tangent and co-tangent space of point **X**. The right side shows tangent and co-tangent space for the current domain and a point **x**. The spatial stretch $\lambda$ is defined by mapping a material element **M** to the current configuration. The maps $\varphi_t$, **F** and $\mathbf{F}^{-\top}$ map tangents **T**, **t** and normals **A**, **a** between the configurations.

In Eq. (1.23b), the cofactor of **F** given by $\mathrm{cof}(\mathbf{F}) = J\,\mathbf{F}^{-\top}$ maps normals **A** and surface areas $|\mathbf{A}|$ from $\Omega_0$ to the corresponding values **a** and $|\mathbf{a}|$ in $\Omega_t$. Nanson's formula, $\mathrm{d}\mathbf{a} = \mathrm{cof}(\mathbf{F})\,\mathrm{d}\mathbf{A}$, is used to transform surface integrals from Eulerian to Lagrangian description. Note that tangents at a point **X** live in the tangent space $T_{\mathbf{X}}\Omega_0$ and normals live in the co-tangent space $T^*_{\mathbf{X}}\Omega_0$.

Equation (1.23c) describes the volume map from $\Omega_0$ to $\Omega_t$, which simply scales the reference volume $V$ by the determinant $J$ to obtain the volume $v$ in the current configuration.

Furthermore, the deformation gradient **F** is used to define the right Cauchy Green tensor $\mathbf{C} = \mathbf{F}^{\top}\mathbf{F}$, which maps from tangent to co-tangent space in reference configuration, and subsequently the Green-Lagrange strain tensor:

$$\mathbf{E} = \frac{1}{2}(\mathbf{C} - \mathbf{I}).$$

This strain measure can be interpreted as comparing the current Lagrangian metric **C**,

a measure for the symmetric part of the current deformation, with the reference metric which is the identity. Using Eq. (1.22), the Green-Lagrange strain tensor can be formulated in terms of derivatives of the displacements:

$$\mathbf{E} = \frac{1}{2}\left((\nabla \mathbf{U})^\top + \nabla \mathbf{U} + \nabla \mathbf{U}^\top \nabla \mathbf{U}\right). \tag{1.24}$$

In case of small displacements, a simplification is to not distinguish between reference and current configuration. The strain expression given in Eq. (1.24) can be linearized by neglecting products of the derivatives and using the spatial displacements $\mathbf{u}$ instead of $\mathbf{U}$. As a result, the linearized strain tensor $\boldsymbol{\varepsilon}$ is given by:

$$\boldsymbol{\varepsilon} = \frac{1}{2}\left((\nabla \mathbf{u})^\top + \nabla \mathbf{u}\right). \tag{1.25}$$

It can be used together with linear material models to derive a completely linear model.

### 1.2.2 Stress Measures

Continuum mechanical models establish equations for the unknown displacement function $\mathbf{u}$ and its evolution in time via relations between stresses and strains. In the following, we introduce the required stress measures.

The Cauchy stress tensor $\boldsymbol{\sigma}$ results from Euler's cut principle: we consider the mechanical action on an arbitrary, virtual cut out of the body in current configuration. The contact forces on the cut surface at a point $\mathbf{x}$ are described by the traction force $\mathbf{t}$. The traction vector acts on the current configuration and is a function of the position $\mathbf{x} \in \Omega_t$ and the local orientation of the cut given by the normal vector $\mathbf{n}$. Cauchy's theorem states that this relation is linear and the corresponding factors define the second order stress tensor $\boldsymbol{\sigma}$ as follows:

$$\mathbf{t} = \boldsymbol{\sigma} \cdot \mathbf{n}. \tag{1.26}$$

Thus, the Cauchy stress describes the "true stress" of contact forces per deformed surface area. Both slots of the second order tensor are associated with the current configuration. More specifically, $\boldsymbol{\sigma}$ is contravariant and maps from a normal $\mathbf{n}$ in co-tangent space $T^*_{\mathbf{x}}\Omega_t$ to the traction $\mathbf{t}$ in tangent space $T_{\mathbf{x}}\Omega_t$.

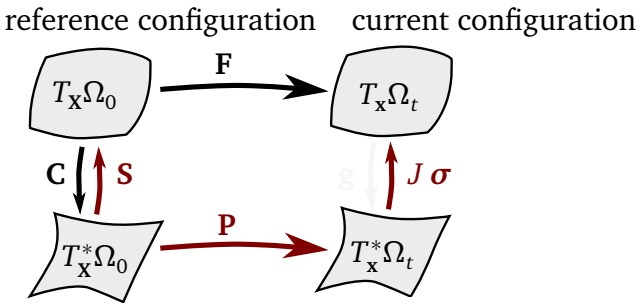


Figure 1.5: Stress tensors and geometric maps that can be used together in a solid mechanics formulation. The right Cauchy-Green tensor $\mathbf{C}$ and the second Piola-Kirchhoff stress $\mathbf{S}$ are dual Eulerian tensors and map between tangent space $T_X\Omega_0$ and co-tangent space $T_X^*\Omega_0$ in the reference domain. The deformation gradient $\mathbf{F}$ and the first Piola-Kirchhoff stress $\mathbf{P}$ are dual two-point tensors mapping from the reference to the current configuration. The Cauchy stress $\boldsymbol{\sigma}$ is defined entirely in the Eulerian setting.

While the physical description is natural in this Eulerian setting, the numerical treatment is more convenient in the Lagrangian setting, where we can integrate over a non-deforming domain. Moreover, a two-point setting, where surface areas are measured in the undeformed configuration and traction forces are measured in the deformed configuration, is often useful in engineering. This is the natural setting, e.g., in tension tests. Therefore, other stress measures involving the reference configuration are defined.

Using the mappings presented in Eq. (1.23), all quantities can be transformed between both configurations. The physical derivation can be carried out equivalently in a Lagrangian or Eulerian setting and switching between them is possible at any point in the derivation. For this purpose, two operations are defined: the pull-back $\varphi^*(\mathbf{a}) = \mathbf{F}^\top \mathbf{a}\,\mathbf{F}$ and push-forward operations $\varphi_*(\mathbf{A}) = \mathbf{F}^{-\top}\mathbf{A}\,\mathbf{F}^{-1}$, which bring tensors from Eulerian to Lagrangian description and vice-versa.

The first Piola-Kirchhoff stress tensor $\mathbf{P}$ measures contact forces in the current configuration with regard to the area of the reference configuration and relates to the Cauchy stress as $\mathbf{P} = \boldsymbol{\sigma}\,\mathrm{cof}(\mathbf{F})$. The second Piola-Kirchhoff tensor $\mathbf{S}$ is a fully Lagrangian field given as the pull-back of the Cauchy stress scaled by $J$:

$$\mathbf{S} = \varphi^*(J\,\boldsymbol{\sigma}) = J\,\mathbf{F}^{-1}\boldsymbol{\sigma}\,\mathbf{F}^{-\top}.$$

Figure 1.5 summarizes the geometric maps by black arrows and the stress measures by red arrows. The Lagrangian setting defines the right Cauchy-Green tensor $\mathbf{C}$ and the second Piola-Kirchhoff stress tensor $\mathbf{S}$. We use these quantities in the derivation of the

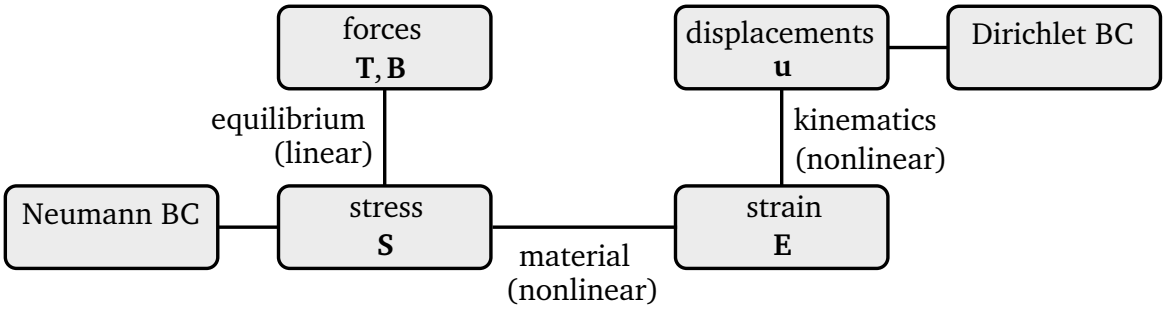


Figure 1.6: The three relations between various quantities that compose the solid mechanics model: Equilibrium links traction and body forces **T** and **B** to the stresses **S**. A material model connects them to strains **E**. The kinematic relations yield the resulting displacement field **u**. Note that all quantities in this diagram are given in Lagrangian formulation.

discretized equations, because the Lagrangian formulation is natural for this task and allows to integrate over the non-deforming domain $\Omega_0$.

The Cauchy stress $\boldsymbol{\sigma}$ is completely defined in the Eulerian setting. It is used to formulate physical balance principles.

### 1.2.3 Overview of the Physical Relations

The previously introduced quantities are linked together by various relations, which are summarized in the digram in Fig. 1.6. The goal is to find the relationship between given forces (top left in Fig. 1.6) and the resulting deformation of the body described by the displacements (top right in Fig. 1.6). Prescribed external traction forces **T** and external or inertial body forces **B** act on the body and result in stresses **S** satisfying the *equilibrium* relation. A *material law* connects stresses **S** and strains **E**. The *kinematics* of the body determine the relationship between displacements **u** and strains **E**. Geometric Dirichlet boundary conditions prescribe displacements and Neumann boundary conditions such as traction forces contribute to the stress field.

Whereas the equilibrium relation is linear, the material and kinematic descriptions can both be chosen to be linear or nonlinear. In cases of small strains, geometric and material linearity can be assumed. We derive two such formulations: a linear formulation where all relations are linear and a nonlinear formulation with nonlinear material and kinematic relations.

### 1.2.4 Assumptions and Model Equations

The foundation of continuum mechanics usually builds on three balance principles: conservation of mass, of momentum and of angular momentum. In the following, these principles are presented in their Eulerian forms.

First, we assume *conservation of mass* in terms of the densities $\rho_0(\mathbf{X})$ and $\rho(\mathbf{x})$ in reference and current configurations:

$$\int_{V_0} \rho_0 \, \mathrm{d}V = \int_{V_t} \rho \, \mathrm{d}v.$$

The equation holds for all corresponding subdomains $V_0 \subset \Omega_0$ and $V_t \subset \Omega_t$. With the intermediate step of deducing $\mathrm{d}/\mathrm{d}t \int_{\Omega_t} \rho \, \mathrm{d}v = 0$, we get the following differential equation:

$$\dot{\rho}(\mathbf{v}, t) + \rho(\mathbf{x}, t) \operatorname{div}\big(\mathbf{v}(\mathbf{x}, t)\big) = 0. \tag{1.27}$$

As muscle tissue largely consists of water, it is typically assumed to be an incompressible domain. This is equivalent to a constant density, $\dot{\rho} = 0$, and, thus, Eq. (1.27) reduces to

$$\operatorname{div}(\mathbf{v}(\mathbf{x}, t)) = 0. \tag{1.28}$$

The second assumption is the *balance of momentum*, which is expressed as

$$\frac{\mathrm{d}}{\mathrm{d}t} \int_{V_t} \rho \, \mathbf{v} \, \mathrm{d}v = \int_{V_t} \rho \, \mathbf{b} \, \mathrm{d}v + \int_{\partial V_t} \mathbf{t} \, \mathrm{d}a. \tag{1.29}$$

Here, $\mathbf{b}$ describes a body force and $\mathbf{t}$ describes a traction force that acts on the surface of the domain $V_t$. Using the Cauchy theorem Eq. (1.26), it can be replaced by the Cauchy stress $\boldsymbol{\sigma}$. The corresponding differential form is given by the following differential equation:

$$\rho \, \dot{\mathbf{v}}(\mathbf{x}, t) = \rho \, \mathbf{b}(\mathbf{x}, t) + \operatorname{div} \boldsymbol{\sigma}(\mathbf{x}, t). \tag{1.30}$$

It relates external forces to the internal stress field and describes the *equilibrium* relation in Fig. 1.6 in Eulerian form. For the discretization, a Lagrangian form is typically used.

For hyperelastic materials, which we consider in the muscle model, the equilibrium relation can also be formulated in terms of the *Hellinger-Reissner energy functional* $\Pi_L(\mathbf{u}, p)$,

which describes the potential energy of the system depending on the displacement and pressure functions $\mathbf{u}$ and $p$. Analogous to the local form in Eq. (1.30), it contains terms for the external loads and for the internal response of the body. The functional is additively composed of external and internal potential energy:

$$\Pi_L(\mathbf{u}, p) = \Pi_{\text{ext}}(\mathbf{u}) + \Pi_{\text{int}}(\mathbf{u}, p). \tag{1.31}$$

The external energy functional is formulated by

$$\Pi_{\text{ext}}(\mathbf{u}) = -\int_{\Omega_0} \mathbf{B}\,\mathbf{u}\,\mathrm{d}V - \int_{\partial\Omega_0^t} \bar{\mathbf{T}}\,\mathbf{u}\,\mathrm{d}S, \tag{1.32}$$

with body force $\mathbf{B}$ in reference configuration and prescribed surface traction $\bar{\mathbf{T}}$ on the traction boundary $\partial\Omega_0^t$. The body force term $\mathbf{B}$ also includes the inertial forces of mass density times acceleration, $\rho\,\dot{\mathbf{v}}$, in case of a dynamic model. The internal energy functional $\Pi_{\text{int}}(\mathbf{u}, p)$ describes the strain energy of the system depending on the displacement field $\mathbf{u}$ and the hydrostatic pressure $p$. The term is defined in Sec. 1.4.2.

The *principle of stationary potential energy* demands that the potential energy functional $\Pi_L$ is stationary. Variational calculus and differentiation of Eq. (1.31) lead to the local Eulerian description given in Eqs. (1.29) and (1.30).

The third assumption is the *balance of angular momentum* and can be formulated using the 3D cross-product:

$$\frac{\mathrm{d}}{\mathrm{d}t}\int_{V_t} \mathbf{x}\times(\rho\,\mathbf{v})\,\mathrm{d}v = \int_{V_t} \mathbf{x}\times(\rho\,\mathbf{b})\,\mathrm{d}v + \int_{\partial V_t} \mathbf{x}\times\mathbf{t}\,\mathrm{d}a.$$

This can be shown to be equivalent to the symmetry of the Cauchy stress tensor, $\boldsymbol{\sigma} = \boldsymbol{\sigma}^\top$.

A further assumption in the multi-scale muscle framework is to only consider isothermal conditions. An activated muscle performs work and energy is added to the system by metabolism. Further, the muscle is not thermodynamically isolated. The system is not closed regarding conversion and transfer of energy and, thus, the balance of energy cannot be modeled easily.

Regarding the required relations to obtain the deformation of the body from external loads given in Fig. 1.6, the *equilibrium* relation is given by Eq. (1.30) and the nonlinear *kinematic* relation is given by Eq. (1.24). The *material* relation has yet to be defined. The mathematical description is closed by defining a constitutive relation between stresses and strains in the next sections.

Section 1.2.5 defines a linear material model that can be used together with linearized kinematics to formulate a fully linear model. Section 1.2.7 presents the nonlinear material model to proceed with the fully nonlinear description.

### 1.2.5 Linear Material Model

For a linear constitutive relation between strain and stress, the linearized strain tensor $\boldsymbol{\varepsilon}$, defined in Eq. (1.25) is used together with the Eulerian Cauchy stress $\boldsymbol{\sigma}$. The generic linear material model is *Hooke*'s law, given by

$$\boldsymbol{\sigma} = \mathbb{C} : \boldsymbol{\varepsilon} \tag{1.33}$$

with the fourth order material tensor

$$\mathbb{C}_{abcd} = K\,\delta_{ab}\,\delta_{cd} + \mu\,(\delta_{ac}\,\delta_{bd} + \delta_{ad}\,\delta_{bc} - \frac{2}{3}\,\delta_{ab}\,\delta_{cd}).$$

The bulk modulus $K$ is a measure for the (in-)compressibility and the shear modulus $\mu$ specifies the elastic shear stiffness. $\delta_{ab}$ is the Kronecker delta. The material tensor $\mathbb{C}$ exhibits the following major and minor symmetries:

$$\mathbb{C}_{abcd} = \mathbb{C}_{cdab}, \qquad \text{(major symmetries)} \tag{1.34a}$$

$$\mathbb{C}_{abcd} = \mathbb{C}_{bacd} = \mathbb{C}_{abdc} = \mathbb{C}_{badc}, \qquad \text{(minor symmetries)} \tag{1.34b}$$

effectively reducing the number of independent entries from 81 to 21 for 3D domains.

To incorporate force generation in the muscle, the stress can be additively composed of a the passive stress $\boldsymbol{\sigma}$ and an additional active stress term $\boldsymbol{\sigma}_{\text{active}}$:

$$\boldsymbol{\sigma}^{\text{total}} = \boldsymbol{\sigma} + \boldsymbol{\sigma}^{\text{active}}. \tag{1.35}$$

### 1.2.6 Nonlinear Material Modeling

Next, we present the derivation of a nonlinear model that does not make any linearization assumptions of small strains as in the previous section. We begin with the description of the material law, which links strains and stresses.

The scalar strain energy function $\Psi$ describes the elastic energy of the material depending on the deformation. The definition of $\Psi$ suffices to describe the behavior of a hyperelastic material. The strain energy function links the right Cauchy Green tensor $\mathbf{C}$ to the second Piola-Kirchhoff stress tensor $\mathbf{S}$ by the relation

$$\mathbf{S} = 2\frac{\partial \Psi(\mathbf{C})}{\partial \mathbf{C}}. \tag{1.36}$$

The *principle of material objectivity* requires that material properties are invariant under a change of observer. As a result, the *representation theorem for isotropic materials* states that the stress tensor can be represented using three strain invariants $I_1, I_2$ and $I_3$. For a transversely isotropic material, two invariants $I_4$ and $I_5$ that depend on the anisotropy direction $\mathbf{a}_0$ (corresponding to a fiber direction) are added. Consequently, we can formulate the strain energy function $\Psi = \Psi(I_1, I_2, I_3, I_4, I_5)$ in terms of these invariants. The principle strain invariants $I_1$ to $I_3$ of the right Cauchy-Green tensor $\mathbf{C}$ and the additional anisotropic invariants $I_4$ and $I_5$ are defined as:

$$I_1(\mathbf{C}) = \mathrm{tr}\,(\mathbf{C}), \qquad I_2(\mathbf{C}) = \frac{1}{2}\left(\mathrm{tr}\,(\mathbf{C})^2 - \mathrm{tr}\,(\mathbf{C}^2)\right), \qquad I_3(\mathbf{C}) = \det(\mathbf{C}) = J^2,$$

$$I_4(\mathbf{C}, \mathbf{a}_0) = \mathbf{a}_0 \cdot \mathbf{C}\,\mathbf{a}_0, \qquad I_5(\mathbf{C}, \mathbf{a}_0) = \mathbf{a}_0 \cdot \mathbf{C}^2\,\mathbf{a}_0.$$

The fiber stretch is related to the fourth invariant by $\lambda_f = \sqrt{I_4}$. Note that requiring incompressibility is equivalent to enforcing $J = 1$, and, in this case, we get $I_3(\mathbf{C}) = 1$.

It is convenient to use a decoupled description, where the deformation gradient $\mathbf{F}$ and the right Cauchy-Green tensor $\mathbf{C}$ are multiplicatively decomposed into volume-changing (volumetric) and volume-preserving (isochoric) parts:

$$\mathbf{F} = (J^{1/3}\mathbf{I})\,\bar{\mathbf{F}}, \qquad \mathbf{C} = (J^{2/3}\mathbf{I})\,\bar{\mathbf{C}}.$$

Here, the volumetric parts are the identity tensors scaled by a power of the determinant $J$ of the deformation gradient. The isochoric or distortional parts $\bar{\mathbf{F}}$ and $\bar{\mathbf{C}}$ are given by

$$\bar{\mathbf{F}} = J^{-1/3}\,\mathbf{F}, \qquad \bar{\mathbf{C}} = J^{-2/3}\,\mathbf{C}. \tag{1.37}$$

The reduced invariants $\bar{I}_1$ to $\bar{I}_5$ of the reduced right Cauchy-Green tensor $\bar{\mathbf{C}}$ are defined accordingly. Similarly, the strain energy function has a decoupled representation with

volumetric part $\Psi_{\text{vol}}$ and isochoric part $\Psi_{\text{iso}}$:

$$\Psi = \Psi_{\text{vol}}(J) + \Psi_{\text{iso}}(\bar{\mathbf{C}}) = \Psi_{\text{vol}}(J) + \Psi_{\text{iso}}(\bar{I}_1, \bar{I}_2, \bar{I}_4, \bar{I}_5). \tag{1.38}$$

Using the decoupled form, any incompressible material can be modeled with the *penalty method* as follows. The material behaviour is given by the isochoric strain energy $\Psi_{\text{iso}}(\bar{\mathbf{C}})$, e.g., by employing the Mooney-Rivlin model in Eq. (1.39). The volumetric part is defined as

$$\Psi_{\text{vol}}(J) = \kappa\, G(J) \qquad \text{with } G(J) = \frac{1}{2}(J-1)^2,$$

with the incompressibility parameter $\kappa$ and the penalty function $G(J)$. This function is strictly convex and approaches zero as $J$ approaches 1. For large values of $\kappa$, the behavior is nearly incompressible. A disadvantage of this method is, that the resulting system becomes singular for $J \to 1$.

A better approach in this regard is to use a mixed formulation, where incompressibility is enforced exactly using a Lagrange multiplier. This approach is also implemented in OpenDiHu and is the preferred method for incompressible materials.

In OpenDiHu, the strain energy function of a new material can be given using the following four terms:

$$\Psi = \Psi_{\text{vol}}(J) + \Psi_{\text{iso}}(\bar{I}_1, \bar{I}_2, \bar{I}_4, \bar{I}_5) + \Psi_1(I_1, I_2, I_3) + \Psi_2(\mathbf{C}, \mathbf{a}_0).$$

The decoupled form is available with $\Psi_{\text{vol}}$ and $\Psi_{\text{iso}}$, the coupled form for isotropic materials can be used via $\Psi_1$. The term $\Psi_2$ gives the most flexibility, as the constitutive model can be directly formulated using the right Cauchy-Green tensor $\mathbf{C}$ and the fiber direction $\mathbf{a}_0$. The unused terms among $\Psi_{\text{vol}}, \Psi_{\text{iso}}, \Psi_1$ and $\Psi_2$ can be defined as constant zero. The incompressibility constraint using Lagrange multipliers can be switched on or off such that both incompressible and compressible materials can be computed.

### 1.2.7 The Nonlinear Material Model for Muscle Contraction

In the muscle contraction model of [Hei13], the strain energy function is additively composed of two passive terms, one isotropic, one anisotropic, and one additional active

term:

$$\Psi(\mathbf{C}) = \Psi_{\text{isotropic}}(I_1, I_2) + \Psi_{\text{anisotropic}}(\lambda_f) + \Psi_{\text{active}}(\gamma).$$

The isotropic term $\Psi_{\text{isotropic}}$ is formulated in terms of the strain invariants $I_1 = \text{tr}(\mathbf{C})$ and $I_2 = \left(\text{tr}(\mathbf{C})^2 - \text{tr}(\mathbf{C}^2)\right)/2$. The anisotropic term $\Psi_{\text{anisotropic}}$ depends on the fiber stretch $\lambda_f$. The active term $\Psi_{\text{active}}$ yields the active stress that results from muscular activation, which is described by the activation parameter $\gamma$.

The passive behavior of muscle tissue is modeled by a transversely isotropic Mooney-Rivlin material. The isotropic part is given by the Mooney-Rivlin formulation:

$$\Psi_{\text{isotropic}}(I_1, I_2) = c_1 (I_1 - 3) + c_2 (I_2 - 3). \tag{1.39}$$

The values of the two material parameters $c_1$ and $c_2$ can be determined by compression tests and are summarized in the work of [Hei13].

The anisotropic behavior depends only on the fiber stretch $\lambda_f$. The formulation in [Hei13] uses two material parameters $b$ and $d$ and the following function:

$$\Psi_{\text{anisotropic}}(\lambda_f) = \frac{b}{d}(\lambda_f^d - 1) - b \log(\lambda_f).$$

The active contribution is directly formulated in terms of the second Piola-Kirchhoff stress $\mathbf{S}$. The relation between the active stress $\mathbf{S}_{\text{active}}$ and the active contribution $\Psi_{\text{active}}$ of the strain energy function as well as the definition of $\mathbf{S}_{\text{active}}$ is given as follows:

$$\mathbf{S}_{\text{active}} = \frac{1}{\lambda_f} \frac{\partial \Psi_{\text{active}}}{\partial \lambda_f} \mathbf{A} \otimes \mathbf{A} = \frac{1}{\lambda_f} \cdot S_{\text{max,active}} \cdot f_\ell(\lambda_f) \cdot \bar{\gamma}\, \mathbf{A} \otimes \mathbf{A}. \tag{1.40}$$

Here, the resulting active stress tensor $\mathbf{S}_{\text{active}}$ is the second order tensor oriented according to the material fiber direction $\mathbf{A} : \Omega_0 \to \mathbb{R}^3$ and given by the dyadic product $\mathbf{A} \otimes \mathbf{A} = A_i A_j\, \mathbf{e}_i \otimes \mathbf{e}_j$, scaled by the maximum active stress parameter $S_{\text{max,active}}$, a function $f_\ell$ that models the force-length relation, and the 3D homogenized value $\bar{\gamma}$ of the activation parameter $\gamma \in [0, 1]$ following from the half-sarcomere model.

In the deforming body fat layer, the active stress contribution is disregarded. For simulating tendons, different material models can be used such as the model proposed by Carniel et al. [Car17], which describes microstructural interactions between collagen fibers and their matrix in addition to the elastic response of the fibers themselves. To alter

the material model, the definition of $\Psi$ can simply be changed while all other equations of the solid mechanics model remain intact.

### 1.2.8 Summary of the Solid Mechanics Model Equations

In summary, the model of solid mechanics for muscle contraction is solved for the unknown displacements $\mathbf{u}$ and additionally the velocities $\mathbf{v}$ if a dynamic formulation is considered.

The model equations follow from the following balance principles:

$$\operatorname{div}(\mathbf{v}) = 0, \qquad \text{(incompressibility)} \tag{1.41a}$$

$$\rho\,\dot{\mathbf{v}} = \rho\,\mathbf{b} + \operatorname{div}\boldsymbol{\sigma}, \qquad \text{(balance of linear momentum)} \tag{1.41b}$$

$$\boldsymbol{\sigma} = \boldsymbol{\sigma}^{\top}, \qquad \text{(balance of angular momentum)} \tag{1.41c}$$

with the constant density $\rho$, external body forces $\mathbf{b}$ and the Cauchy stress tensor $\boldsymbol{\sigma}$.

Additionally, geometric relations between displacements $\mathbf{u}$ and strains $\mathbf{E}$ or $\boldsymbol{\varepsilon}$ are assumed, either fully nonlinear in Eq. (1.24) or with corresponding linearization assumptions in Eq. (1.25). Furthermore, a material model is given that relates strains and stresses. A linear model is described in Sec. 1.2.5. The framework for nonlinear hyperelastic models uses a strain energy function $\Psi$ as described in Sec. 1.2.6. A particular nonlinear material model for muscle contraction from the literature is described in Sec. 1.2.7.

The description of the multi-scale model [Röh12]; [Hei13] assumes quasi-static conditions, which means that the velocities are set to zero, $\mathbf{v} = \mathbf{0}$, and inertial terms are neglected. As a consequence, the incompressibility constraint in Eq. (1.41a) has to be formulated differently and the balance of momentum in Eq. (1.41b) reduces to $\rho\,\mathbf{b} + \operatorname{div}\boldsymbol{\sigma} = 0$. Our implementation extends the model to the fully dynamic formulation given in Equations (1.41a) to (1.41c).

Initial conditions for the displacements $\mathbf{u}$ and velocities $\mathbf{v}$ define the initial pose of the muscle tissue:

$$\mathbf{u}(\mathbf{x},0) = \mathbf{u}_0(\mathbf{x}), \qquad \mathbf{v}(\mathbf{x},0) = \mathbf{v}_0(\mathbf{x}) \qquad \text{for } \mathbf{x} \in \Omega_M.$$

Dirichlet boundary conditions for $\mathbf{u}$ and $\mathbf{v}$ can fix certain parts of the muscle, e.g., at the attachment points of the tendons:

$$\mathbf{u}(\mathbf{x}, t) = \bar{\mathbf{u}}(t), \qquad \mathbf{v}(\mathbf{x}, t) = \bar{\mathbf{v}}(t) \qquad \text{for } \mathbf{x} \in \partial\Omega_{\text{Dirichlet}}.$$

Additionally, Neumann boundary conditions can be used to prescribe traction forces on the surface.

The derivation of the Finite Element formulation and the resulting numerical scheme to obtain the solution functions $\mathbf{u}$ and $\mathbf{v}$ are discussed in Sec. 1.4.

## 1.3 Discretization

The partial and ordinary differential equations described in the last section contain spatial and temporal derivatives that have to be discretized to be solved numerically. For temporal derivatives, we use timestepping schemes, for spatial derivatives, we employ the Finite Element Method.

In this section, we describe the discretization of the subcellular and electrophysiology models that were presented in the last section. A description of the discretization of the solid mechanics model follows in Sec. 1.4.

We begin with the discretization in time in Sec. 1.3.1, followed by the spatial discretization for the monodomain (Sections 1.3.2 and 1.3.3) and multidomain models (Sections 1.3.4 and 1.3.5).

### 1.3.1 Discretization of the Monodomain Model

Electrophysiology models typically consists of a reaction-diffusion equation. The diffusion term describes the electric conduction in the tissue and the reaction term includes the subcellular model. In our model, the monodomain equation Eq. (1.11) used in the fiber based description and the second multidomain equation Eq. (1.15) are equations of this type.

This type of partial differential equation is often solved using operator splitting schemes. A first order operator splitting scheme is Godunov splitting [Gui03]. It was used for the

solution of the chemo-electro-mechanical model in [Röh12]. In addition to Godunov splitting, we also employ the second order accurate Strang splitting scheme [Str68].

In the following, the application of these two schemes is illustrated for the monodomain equation Eq. (1.11). The right hand sides of the diffusion and reaction terms are denoted in short as $\mathcal{L}_1$ and $\mathcal{L}_2$:

$$\mathcal{L}_1(V_m) := \frac{1}{A_m C_m} \sigma_{\text{eff}} \frac{\partial^2 V_m}{\partial x^2}, \qquad \mathcal{L}_2(V_m) := -\frac{1}{C_m} I_{\text{ion}}(V_m, \mathbf{y}).$$

Then, the monodomain equation takes the form:

$$\frac{\partial V_m}{\partial t} = \mathcal{L}_1(V_m) + \mathcal{L}_2(V_m). \tag{1.42}$$

A timestepping scheme is constructed that starts with a given initial value $V_m^{(0)}$ and computes solution values $V_m^{(i)}$ at discrete points in time $t^{(i)} = i \cdot dt$ with a fixed timestep width $dt$. Godunov splitting proceeds by alternatingly performing steps in the two directions of the right hand sides $\mathcal{L}_1$ and $\mathcal{L}_2$. In the first substep per iteration, an intermediate value $V_m^*$ is calculated, which is used as starting point for the second substep. Each of the substeps are performed using independent timestepping scheme, e.g., the explicit Euler scheme:

$$V_m^* = V_m^{(i)} + dt\, \mathcal{L}_1(V_m^{(i)}, t^{(i)}), \tag{1.43a}$$

$$V_m^{(i+1)} = V_m^* + dt\, \mathcal{L}_2(V_m^*, t^{(i)}) \tag{1.43b}$$

Strang splitting uses a similar approach with three substeps per timestep and two intermediate values $V_m^*$ and $V_m^{**}$:

$$V_m^* = V_m^{(i)} + \frac{dt}{2} \mathcal{L}_1(V_m^{(i)}, t^{(i)}), \tag{1.44a}$$

$$V_m^{**} = V_m^* + dt\, \mathcal{L}_2(V_m^*, t^{(i)}), \tag{1.44b}$$

$$V_m^{(i+1)} = V_m^{**} + \frac{dt}{2} \mathcal{L}_1(V_m^{**}, t_{(i)} + \frac{1}{2} dt). \tag{1.44c}$$

Note that each substep can either be executed as a single timestep of the chosen method as in Eqs. (1.43) and (1.44) or divided into several steps with timestep widths $dt_{0D}$ (for the

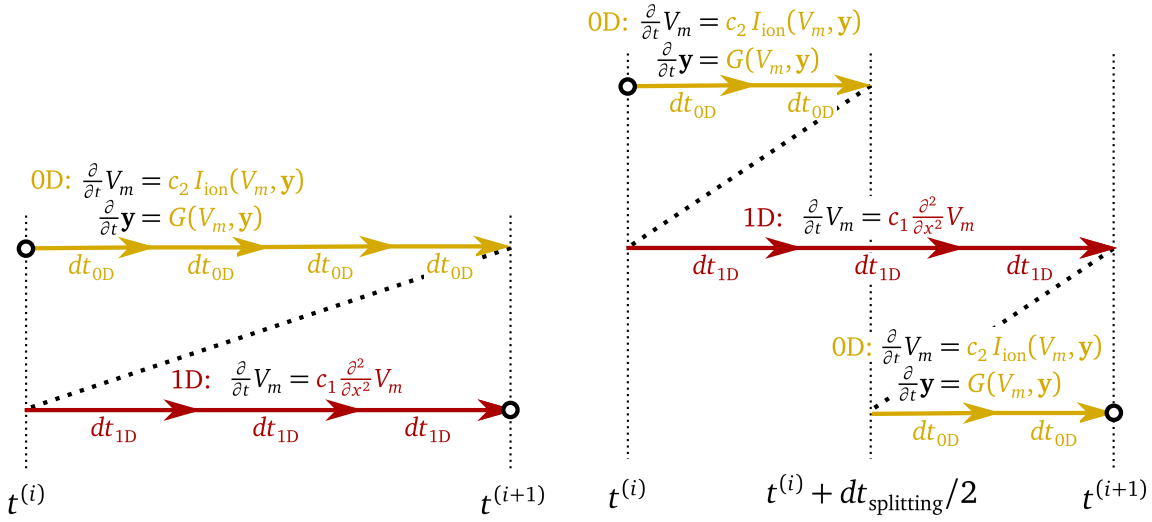


(a) The Godunov splitting uses two substeps: 0D, 1D.

(b) The Strang splitting uses three substeps: 0D, 1D, 0D.

Figure 1.7: Godunov and Strang splitting schemes that are used to solve the monodomain equation. The equation is split into a reaction part (0D,yellow) and a diffusion part (1D,red) and these parts are solved alternatingly. The visualizations show one splitting timestep starting at the left circle and completing at the right circle.

0D subcellular model represented by $\mathcal{L}_1$) and $dt_{1D}$ (for the diffusion equation represented by $\mathcal{L}_2$).

Figure 1.7 visualizes both splitting schemes applied to the monodomain equation. The yellow arrows correspond to the solution of the 0D subcellular model. The red arrows correspond to the solution of the 1D diffusion equation. The timestep width of one splitting step is $dt_{\text{splitting}}$. Depending on how the timestep widths are chosen in relation to each other, different numbers of subcycles are used in the solution of the 0D and 1D problems.

Instead of the explicit Euler method in Eqs. (1.43) and (1.44), other timestepping methods can be used for the substeps. We use the following schemes, which are listed as

single steps for the generic ODE $\partial V_m/\partial t = \mathcal{L}(V_m, t)$:

$$V_m^{(i+1)} = V_m^{(i)} + dt\,\mathcal{L}(V_m^{(i)}, t^{(i)}), \tag{1.45a}$$

$$V_m^{(i+1)} = V_m^{(i)} + \frac{dt}{2}\left(\mathcal{L}(V_m^{(i)}, t^{(i)}) + \mathcal{L}\left(V_m^{(i)} + dt\,\mathcal{L}(V_m^{(i)}, t^{(i)}), t^{(i+1)}\right)\right), \tag{1.45b}$$

$$V_m^{(i+1)} = V_m^{(i)} + dt\,\mathcal{L}(V_m^{(i+1)}, t^{(i+1)}), \tag{1.45c}$$

$$V_m^{(i+1)} = V_m^{(i)} + \frac{dt}{2}\left(\theta\,\mathcal{L}(V_m^{(i+1)}, t^{(i+1)}) + (1-\theta)\,\mathcal{L}(V_m^{(i)}, t^{(i)})\right). \tag{1.45d}$$

Here, Eq. (1.45a) is the first-order accurate explicit Euler scheme, Eq. (1.45b) is the second-order accurate Heun scheme, Eq. (1.45c) is the first order accurate implicit Euler scheme, and Eq. (1.45d) is the Crank-Nicolson scheme [Cra47], which for $\theta = 0$ equals the explicit Euler and for $\theta = 1$ equals the implicit Euler scheme. For $\theta = \frac{1}{2}$, it is second order accurate. An advantage of the implicit schemes in Eqs. (1.45c) and (1.45d) is, that, for our considered diffusion problems, they are unconditionally stable. A disadvantage is, that a linear equation has to be solved in every timestep.

A second order accurate timestepping scheme yields a faster decrease of the numerical error with decreasing step size and, thus, in many cases allows a larger step size than a first order scheme. To obtain a second order scheme for the monodomain equation, we use Strang splitting (Eq. (1.44)) with the Crank-Nicolson scheme (Eq. (1.45d)) for the diffusion term $\mathcal{L}_1$ and Heun's method (Eq. (1.45b)) for the reaction term $\mathcal{L}_2$. In the subcellular model, the system of ODEs with state vector $\mathbf{y}$ given in Eq. (1.6) is solved with Heun's method along with the equation in terms of $V_m$.

Next, the spatial derivatives in the diffusion part $\mathcal{L}_2$ of the split equation have to be discretized. Then, both the multidomain and the fiber based models can be solved using the splitting scheme.

### 1.3.2 Discretization of the Diffusion and Laplace Equations

For the spatial discretization, we first derive the Finite Element formulation for a generic parabolic diffusion equation in a domain $\Omega \subset \mathbb{R}^d$ of arbitrary dimensionality $d$. Then, specialization to 1D yields the formulation for the monodomain equation. Considering a 3D domain, the formulation is an important building block for the discretization of the multidomain model. This is shown in more detail in a later section, Sec. 1.3.4

We consider the following diffusion problem in the variable $u : \Omega \times [0, t_{\text{end}}] \to \mathbb{R}$ with Neumann boundary conditions on a part of the boundary $\Gamma_f \subset \partial\Omega$ with normal vector $\mathbf{n}$:

$$\frac{\partial u}{\partial t} = \operatorname{div}(\boldsymbol{\sigma} \operatorname{grad} u), \quad (\boldsymbol{\sigma} \operatorname{grad} u) \cdot \mathbf{n} = f \quad \text{on } \Gamma_f, \quad (\boldsymbol{\sigma} \operatorname{grad} u) \cdot \mathbf{n} = 0 \quad \text{on } \partial\Omega \backslash \Gamma_f.$$

We discretize the temporal derivative using the Crank-Nicolson scheme as in Eq. (1.45d). Following the procedure of the Galerkin Finite Element formulation with the Hilbert space $H_0^1(\Omega)$ of test functions $\phi$ that are zero on the boundary, we arrive at the following weak form:

$$\int_\Omega \left(\theta \nabla \cdot (\boldsymbol{\sigma} \nabla \mathbf{u}^{(i+1)}) + (1-\theta) \nabla \cdot (\boldsymbol{\sigma} \nabla u^{(i)})\right) \phi \, \mathrm{d}\mathbf{x} \\ = \frac{1}{dt} \int_\Omega (u^{(i+1)} - u^{(i)}) \, \phi \, \mathrm{d}\mathbf{x}, \qquad \forall \phi \in H_0^1(\Omega).$$

For brevity, we express divergence and gradient using the nabla operator.

To discretize the weak form in space, we choose a function space $V_h = \operatorname{span}\{\varphi_j \mid j = 1, \ldots, N\}$ to represent the solution as $u = \sum_{j=1}^N u_j \phi_j$. Applying the divergence theorem, we obtain:

$$\sum_{j=1}^N \left(\theta \, u_j^{(i+1)} + (1-\theta) u_j^{(i)}\right) \left(-\int_\Omega \boldsymbol{\sigma} \nabla \varphi_j \cdot \nabla \varphi_k \, \mathrm{d}\mathbf{x} + \int_{\partial\Omega} \left(\boldsymbol{\sigma} \nabla \varphi_j \cdot \mathbf{n}\right) \varphi_k \, \mathrm{d}\mathbf{x}\right) \\ = \frac{1}{dt} \sum_{j=1}^N \left(u_j^{(i+1)} - u_j^{(i)}\right) \int_\Omega \varphi_j \, \varphi_k \, \mathrm{d}\mathbf{x}, \qquad \forall k = 1, \ldots, N. \tag{1.46}$$

This iteration step can be written in matrix notation in terms of the vectors of unknowns $\mathbf{u}^{(i)} = (u_0^{(i)}, \ldots, u_N^{(i)})^\top$ at timestep $i$:

$$\mathbf{A}\,\mathbf{u}^{(i+1)} = \mathbf{b}(\mathbf{u}^{(i)}).$$

The system matrix $\mathbf{A}$ and the right hand side $\mathbf{b}$ are given by:

$$\mathbf{A} = \theta\,(\mathbf{K}_\sigma + \mathbf{B}_\sigma) - \frac{1}{dt}\mathbf{M}, \qquad \mathbf{b} = \left((\theta - 1)\,(\mathbf{K}_\sigma + \mathbf{B}_\sigma) - \frac{1}{dt}\mathbf{M}\right)\mathbf{u}^{(i)}.$$

The formulation uses the standard stiffness matrix $\mathbf{K}_\sigma$, the matrix $\mathbf{B}_\sigma$ of the boundary

integral and the mass matrix $\mathbf{M}$, whose components are defined as

$$\mathbf{K}_{\boldsymbol{\sigma},kj} = -\int_\Omega (\boldsymbol{\sigma}\,\nabla\varphi_j)\cdot\nabla\varphi_k\,\mathrm{d}\mathbf{x}, \quad \mathbf{B}_{\boldsymbol{\sigma},kj} = \int_{\Gamma_f} \big((\boldsymbol{\sigma}\,\nabla\varphi_j)\cdot\mathbf{n}\big)\,\varphi_k\,\mathrm{d}\mathbf{x}, \quad \mathbf{M}_{kj} = \int_\Omega \varphi_j\,\varphi_k\,\mathrm{d}\mathbf{x}. \tag{1.47}$$

Note that, after applying the divergence theorem, the definition of the stiffness matrix has a minus sign.

Next, we take into account the Neumann boundary condition $\boldsymbol{\sigma}\nabla u\cdot\mathbf{n} = f$ on the boundary $\Gamma_f$. The flux $f$ over the boundary is discretized by $M$ separate ansatz functions $\psi_j$ on $\Gamma_f$ as $f = \sum_{j=1}^{M} f_j\,\psi_j$. The flux values are summarized in a vector $\mathbf{f} = (f_1,\dots,f_M)^\top$. Plugging this into Eq. (1.46) yields the following equation in matrix notation:

$$\tilde{\mathbf{A}}\,\mathbf{u}^{(i+1)} = \tilde{\mathbf{b}}(\mathbf{u}^{(i)}), \tag{1.48}$$

with the system matrix $\tilde{\mathbf{A}}$ and right hand side $\tilde{\mathbf{b}}$:

$$\tilde{\mathbf{A}} = \theta\,\mathbf{K}_{\boldsymbol{\sigma}} - \frac{1}{dt}\mathbf{M}, \qquad \tilde{\mathbf{b}} = \Big((\theta-1)\,\mathbf{K}_{\boldsymbol{\sigma}} - \frac{1}{dt}\mathbf{M}\Big)\,\mathbf{u}^{(i)} - \mathbf{B}_{\Gamma_f}\left(\theta\,\mathbf{f}^{(i+1)} + (1-\theta)\,\mathbf{f}^{(i)}\right),$$

and the boundary matrix $\mathbf{B}_{\Gamma_f}$ given by:

$$\mathbf{B}_{\Gamma_f,kj} = \int_{\Gamma_f} \psi_j\,\varphi_k\,\mathrm{d}\mathbf{x}. \tag{1.49}$$

Note that incorporating the Neumann boundary conditions in the weak form corresponds to the following exchange of the boundary matrices $\mathbf{B}_\sigma$ and $\mathbf{B}_{\Gamma_f}$:

$$\mathbf{B}_\sigma\,\mathbf{u} = \mathbf{B}_{\Gamma_f}\,\mathbf{f}. \tag{1.50}$$

Equation (1.48) is used to solve the diffusion part of the monodomain equation given in Eq. (1.11) after inserting the corresponding constant prefactors.

When deriving or implementing new models or optimizing solver code, it is often beneficial to study certain effects in isolation. It can help to use a toy problem such as the simple Laplace problem $\Delta u = 0$, possibly with Neumann boundary condition $\partial u/\partial\mathbf{n} = f$. By specializing the formulation in Eq. (1.48) accordingly, we obtain the system

$$(\mathbf{K}_\mathrm{I} + \mathbf{B}_\mathrm{I})\,\mathbf{u} = \mathbf{0}$$

for the case without boundary condition (set $\mathbf{B}_\mathbf{I}$ to zero to assume homogenous Neumann boundaries) or

$$\mathbf{K}_\mathbf{I}\,\mathbf{u} = -\mathbf{B}_{\Gamma_f}\,\mathbf{f} \tag{1.51}$$

to include the formulated Neumann boundary condition.

### 1.3.3 Using Mass Lumping for Implicit Timestepping

Implicit timestepping schemes such as implicit Euler or the Crank-Nicoloson scheme for $\theta = \frac{1}{2}$ need to solve a linear equation in every timestep. Assuming homogeneous Neumann boundary conditions for simplicity, the iteration step of the canonical Crank-Nicolson scheme follows from Eq. (1.48):

$$\big(\frac{1}{2}\mathbf{K} - \frac{1}{dt}\mathbf{M}\big)\,\mathbf{u}^{(i+1)} = \big(-\frac{1}{2}\mathbf{K} - \frac{1}{dt}\mathbf{M}\big)\,\mathbf{u}^{(i)} \tag{1.52a}$$

$$\Leftrightarrow \quad (\mathbf{I} - \frac{dt}{2}\,\mathbf{M}^{-1}\mathbf{K})\,\mathbf{u}^{(i+1)} = (\mathbf{I} + \frac{dt}{2}\,\mathbf{M}^{-1}\mathbf{K})\,\mathbf{u}^{(i)}. \tag{1.52b}$$

For the implicit Euler method, we obtain:

$$(\mathbf{K} - \frac{\mathbf{M}}{dt})\,\mathbf{u}^{(i+1)} = -\frac{\mathbf{M}}{dt}\mathbf{u}^{(i)} \tag{1.53a}$$

$$\Leftrightarrow \quad (\mathbf{I} - dt\,\mathbf{M}^{-1}\mathbf{K})\,\mathbf{u}^{(i+1)} = \mathbf{u}^{(i)}. \tag{1.53b}$$

Both iteration steps in Eqs. (1.52a) and (1.52b) and in Eqs. (1.53) and (1.53a) are equivalent, as the second equation follows from the first one by left multiplication of $(-dt\mathbf{M}^{-1})$. In the second equations, the matrices to be multiplied are created by a sum of the unity matrix $\mathbf{I}$ and another matrix term that is scaled by the potentially small timestep width $dt$. For the implicit Euler in Eq. (1.53b), the matrix on the right hand side even reduces to the identity matrix. This is preferred over the first iteration steps in Eqs. (1.52a) and (1.53a) as it leads to better conditioned matrix-vector multiplications.

The required inversions of the mass matrix cannot be carried out explicitly as the inversion would fill in numerous matrix entries and eliminate the sparse structure. This is not feasible for highly resolved meshes with a large number of degrees of freedom. Instead, *mass lumping* is used, where the mass matrix $\mathbf{M}$ is approximated by a diagonal matrix with diagonal entries equal to the row sums in $\mathbf{M}$ [Hin76]. Thus, multiplication

with the inverse mass matrix corresponds to a rescaling of columns by the inverse lumped diagonal entries.

### 1.3.4 Discretization of the Multidomain Model

With the prerequisites of temporal discretization in Sec. 1.3.1 and the Finite Element formulation of a diffusion equation in Sec. 1.3.2, we can now discretize the multidomain model. Since this has not been previously done in literature using the Finite Element Method, the subsequent derivation is more detailed.

The first multidomain equation given in Eq. (1.14) yields the following form after applying the Finite Element derivation in Eq. (1.48):

$$\left(\mathbf{K}_{\boldsymbol{\sigma}_e+\boldsymbol{\sigma}_i}+\mathbf{B}_{\boldsymbol{\sigma}_e+\boldsymbol{\sigma}_i}\right)\boldsymbol{\phi}_e+\sum_{k=1}^{N_{\mathrm{MU}}} f_r^k\left(\mathbf{K}_{\boldsymbol{\sigma}_i^k}+\mathbf{B}_{\boldsymbol{\sigma}_i^k}\right)\mathbf{V}_m^k=0. \tag{1.54}$$

Here, $\boldsymbol{\phi}_e$ and $\mathbf{V}_m^k$ are the vectors of degrees of freedom for the extracellular potential $\phi_e$ and membrane voltage $V_m^k$ of compartment $k$. The matrices are defined by Eq. (1.47) and do not yet include the boundary conditions. The subscripts of the stiffness matrices $\mathbf{K}$ and boundary integral matrices $\mathbf{B}$ refer to the anisotropy tensors that occur in their definitions.

The diffusion part of the second multidomain equation, Eq. (1.15), discretized with Crank-Nicolson, yields the system

$$\mathbf{A}\begin{pmatrix}\mathbf{V}_m^{k,(i+1)}\\ \boldsymbol{\phi}_e^{(i+1)}\end{pmatrix}=\mathbf{b}, \tag{1.55}$$

with the $1\times 2$ block system matrix $\mathbf{A}$ and right hand side vector $\mathbf{b}$ given by:

$$\mathbf{A}=\left[\frac{\theta}{A_m^k C_m^k}\left(\mathbf{K}_{\boldsymbol{\sigma}_i^k}+\mathbf{B}_{\boldsymbol{\sigma}_i^k}\right)-\frac{1}{dt}\mathbf{M}\qquad \frac{\theta}{A_m^k C_m^k}\left(\mathbf{K}_{\boldsymbol{\sigma}_i^k}+\mathbf{B}_{\boldsymbol{\sigma}_i^k}\right)\right], \tag{1.56a}$$

$$\mathbf{b}=\left(\frac{\theta-1}{A_m^k C_m^k}\left(\mathbf{K}_{\boldsymbol{\sigma}_i^k}+\mathbf{B}_{\boldsymbol{\sigma}_i^k}\right)-\frac{1}{dt}\mathbf{M}\right)\mathbf{V}_m^{k,(i)}+\frac{\theta-1}{A_m^k C_m^k}\left(\mathbf{K}_{\boldsymbol{\sigma}_i^k}+\mathbf{B}_{\boldsymbol{\sigma}_i^k}\right)\boldsymbol{\phi}_e^{(i)}. \tag{1.56b}$$

A separate instance of this equation holds for every compartment $k$. Again, the integrals over the boundary are still present in the $\mathbf{B}_{\boldsymbol{\sigma}_i^k}$ matrices. To resolve this and to close the

formulation, we have to consider the fluxes over the boundary of all involved unknowns and to replace them using the boundary conditions.

One required boundary conditions to solve the multidomain model without body domain is given in Eq. (1.16a). The boundary condition for compartment $k$ in terms of the intracellular potential $\phi_i^k$,

$$(\boldsymbol{\sigma}_i^k \nabla \phi_i^k) \cdot \mathbf{n}_m = 0 \qquad \text{on } \partial\Omega_M, \tag{1.57}$$

is expressed in terms of the unknowns $V_m^k$ and $\phi_e$ to yield the condition

$$(\boldsymbol{\sigma}_i^k \nabla V_m^k) \cdot \mathbf{n}_m = -(\boldsymbol{\sigma}_i^k \nabla \phi_e) \cdot \mathbf{n}_m =: p^k \qquad \text{on } \partial\Omega_M. \tag{1.58}$$

We define the value of this flux to be equal to a helper variable $p^k$. A second flux is formulated for the extracellular potential $\phi_e$. We assign its value to the helper variable $q$:

$$(\boldsymbol{\sigma}_e \nabla \phi_e) \cdot \mathbf{n}_m =: q \qquad \text{on } \partial\Omega_M. \tag{1.59}$$

We can now express the flux value $\big((\boldsymbol{\sigma}_e + \boldsymbol{\sigma}_i)\nabla\phi_e\big) \cdot \mathbf{n}_m$, which occurs in the discretized first multidomain equation, Eq. (1.54), in terms of the variables $p^k$ and $q$. Using Eqs. (1.57) and (1.58) and the relation $\phi_e = \phi_i^k - V_m^k$, we derive:

$$\big((\boldsymbol{\sigma}_e + \boldsymbol{\sigma}_i)\nabla\phi_e\big) \cdot \mathbf{n}_m = (\boldsymbol{\sigma}_e \nabla\phi_e) \cdot \mathbf{n}_m + (\boldsymbol{\sigma}_i \nabla\phi_e) \cdot \mathbf{n}_m = q - \sum_{k=1}^{N_{\mathrm{MU}}} f_r^k \, p^k. \tag{1.60}$$

We discretize the flux values $p^k$ and $q$ analogously to the Neumann boundary condition flux $f$ in Sec. 1.3.2 and summarize the degrees of freedoms in vectors $\mathbf{p}^k$ and $\mathbf{q}$.

Next, we combine the flux values with the first and second multidomain equation. Plugging the generic relation Eq. (1.50) for boundary integral terms into the discretization of the first multidomain equation, Eq. (1.54), and using the derived flux values in Eqs. (1.58) and (1.60) leads in a first step to the following equation:

$$\mathbf{K}_{\boldsymbol{\sigma}_e+\boldsymbol{\sigma}_i} \boldsymbol{\phi}_e + \mathbf{B}_{\Gamma_M} \Big(\mathbf{q} - \sum_{k=1}^{N_{\mathrm{MU}}} f_r^k \, \mathbf{p}^k\Big) + \sum_{k=1}^{N_{\mathrm{MU}}} f_r^k \Big(\mathbf{K}_{\boldsymbol{\sigma}_i^k} \mathbf{V}_m^k + \mathbf{B}_{\Gamma_M} \, \mathbf{p}^k\Big) = 0.$$

It can be seen that the terms involving $\mathbf{p}^k$ cancel out, such that we get:

$$\mathbf{K}_{\boldsymbol{\sigma}_e+\boldsymbol{\sigma}_i}\,\boldsymbol{\phi}_e + \sum_{k=1}^{N_{\mathrm{MU}}} f_r^k \mathbf{K}_{\boldsymbol{\sigma}_i^k}\,\mathbf{V}_m^k = -\mathbf{B}_{\Gamma_M}\,\mathbf{q}. \tag{1.61}$$

If the multidomain description is used without body fat domain, the boundary condition in Eq. (1.16b) is used and the right hand side in Eq. (1.61) vanishes. If a body domain is considered, the right hand side interacts with the body domain model, which is considered in the next section.

Adding boundary conditions to the discretization of the second multidomain equation proceeds using Eqs. (1.55) and (1.56). Carrying out the analogous procedure to the first multidomain equation, we plug in Eq. (1.50) to yield the matrix equation

$$\mathbf{A}\begin{pmatrix}\mathbf{V}_m^{k,(i+1)}\\ \boldsymbol{\phi}_e^{(i+1)}\end{pmatrix} = \mathbf{b} \tag{1.62}$$

with system matrix $\mathbf{A}$ and right hand side vector $\mathbf{b}$ given by

$$\mathbf{A} = \begin{bmatrix}\dfrac{\theta}{A_m^k C_m^k}\mathbf{K}_{\boldsymbol{\sigma}_i^k} - \dfrac{1}{dt}\mathbf{M} & \dfrac{\theta}{A_m^k C_m^k}\mathbf{K}_{\boldsymbol{\sigma}_i^k},\end{bmatrix}, \tag{1.63}$$

$$\begin{aligned}\mathbf{b} = &\Big(\frac{\theta-1}{A_m^k C_m^k}\mathbf{K}_{\boldsymbol{\sigma}_i^k} - \frac{1}{dt}\mathbf{M}\Big)\mathbf{V}_m^{k,(i)} + \frac{\theta-1}{A_m^k C_m^k}\mathbf{K}_{\boldsymbol{\sigma}_i^k}\boldsymbol{\phi}_e^{(i)}\\ &+ \frac{\theta-1}{A_m^k C_m^k}\mathbf{B}_{\Gamma_M}\mathbf{p}^{k,(i)} - \frac{\theta-1}{A_m^k C_m^k}\mathbf{B}_{\Gamma_M}\mathbf{p}^{k,(i)} - \frac{\theta}{A_m^k C_m^k}\mathbf{B}_{\Gamma_M}\mathbf{p}^{k,(i+1)} + \frac{\theta}{A_m^k C_m^k}\mathbf{B}_{\Gamma_M}\mathbf{p}^{k,(i+1)}.\end{aligned}$$

Again, the boundary terms involving $\mathbf{p}^k$ vanish to yield the following expression for $\mathbf{b}$:

$$\mathbf{b} = \Big(\frac{\theta-1}{A_m^k C_m^k}\mathbf{K}_{\boldsymbol{\sigma}_i^k} - \frac{1}{dt}\mathbf{M}\Big)\mathbf{V}_m^{k,(i)} + \frac{\theta-1}{A_m^k C_m^k}\mathbf{K}_{\boldsymbol{\sigma}_i^k}\boldsymbol{\phi}_e^{(i)}. \tag{1.64}$$

In summary, Eq. (1.61) with $\mathbf{q} = \mathbf{0}$ coupled with $N_{\mathrm{MU}}$ instances of Equations (1.62) to (1.64) comprises the discretization for the multidomain model without body domain. Definitions of the involved stiffness and mass matrices are given in Eq. (1.47).

### 1.3.5 Discretization of the Multidomain Model for Surface EMG

To discretize the multidomain model with the electric potential $\phi_b$ in the body domain, we extend the formulation without body domain in Sec. 1.3.4. The body domain adds the electric potential $\phi_b$ to the vector of unknowns, for which the system has to be solved. As before, we discretize the field using Finite Element ansatz functions and solve for the vector $\boldsymbol{\phi}_b$ of degrees of freedom.

The model for $\phi_b$ is the Laplace equation given in Eq. (1.17) with homogeneous Neumann boundary conditions given in Eq. (1.19). According to Eq. (1.51), the discretized equation is given by

$$\mathbf{K}_{\boldsymbol{\sigma}_b}\,\boldsymbol{\phi}_b = 0. \tag{1.65}$$

In addition, the value of the body potential $\phi_b$ is coupled to the extracellular potential $\phi_e$ in the muscle domain $\Omega_M$ via the coupling conditions on the boundary $\Gamma_M$ given in Eq. (1.18).

We write the discretized and coupled multidomain equations as a linear system of equations in generic block-matrix form:

$$\left[\begin{array}{c|c|c|c} \mathbf{A}^k_{V_m,V_m} & \mathbf{B}^k_{V_m,\phi_e} & & \\ \mathbf{B}^k_{\phi_e,V_m} & \mathbf{B}_{\phi_e,\phi_e} & & \mathbf{B}_{\Gamma_M} \\ \hline & & \mathbf{C}_{\phi_b,\phi_b} & -\mathbf{B}_{\Gamma_M} \\ \hline & \mathbf{I}_{\Gamma_M,\phi_e} & -\mathbf{I}_{\Gamma_M,\phi_b} & \end{array}\right] \left[\begin{array}{c} \mathbf{V}_m^{k,(i+1)} \\ \hline \boldsymbol{\phi}_e^{(i+1)} \\ \hline \boldsymbol{\phi}_b^{(i+1)} \\ \hline \mathbf{q}^{(i+1)} \end{array}\right] = \left[\begin{array}{c} \mathbf{b}^{k,(i)}_{V_m} \\ \hline \mathbf{0} \\ \hline \mathbf{0} \\ \hline \mathbf{0} \end{array}\right]. \tag{1.66}$$

The vector of unknowns consists of the degrees of freedom in the Finite Element formulation at the next timestep $(i+1)$ of the transmembrane voltage $\mathbf{V}_m^{k,(i+1)}$, the extracellular potential $\boldsymbol{\phi}_e^{(i+1)}$, the body potential $\boldsymbol{\phi}_b^{(i+1)}$, and additionally the flux $\mathbf{q}^{(i+1)}$ over the shared boundary $\Gamma_M$ of the muscle and the body domain, which was defined in Eq. (1.59). For illustration purposes, only one compartment, $k = 1$, for one MU, $N_{\text{MU}} = 1$, is considered.

We refer to parts of the matrix in Eq. (1.66) as block rows and block columns according to the given block-structure.

The first block row in the matrix equation is given by the discretized second multidomain equation. Following Eqs. (1.63) and (1.64), the matrices and the right hand side

are given by

$$\mathbf{A}^k_{V_m,V_m} = \frac{\theta}{A^k_m\, C^k_m}\,\mathbf{K}_{\boldsymbol{\sigma}^k_i} - \frac{1}{dt}\,\mathbf{M}, \qquad \mathbf{B}^k_{V_m,\phi_e} = \frac{\theta}{A^k_m\, C^k_m}\,\mathbf{K}_{\boldsymbol{\sigma}^k_i},$$

$$\mathbf{b}^{k,(i)}_{V_m} = \Big(\frac{\theta-1}{A^k_m\, C^k_m}\,\mathbf{K}_{\boldsymbol{\sigma}^k_i} - \frac{1}{dt}\,\mathbf{M}\Big)\mathbf{V}^{k,(i)}_m + \frac{\theta-1}{A^k_m\, C^k_m}\,\mathbf{K}_{\boldsymbol{\sigma}^k_i}\,\boldsymbol{\phi}^{(i)}_e.$$

The second block row describes the first multidomain equation that was derived in Eq. (1.61). The flux term $\mathbf{q}$ has been brought to the left hand side and is incorporated by the boundary matrix $\mathbf{B}_{\Gamma_M}$ defined in Eq. (1.49). The other matrices are formulated as follows:

$$\mathbf{B}^k_{\phi_e,V_m} = f^k_r \mathbf{K}_{\boldsymbol{\sigma}^k_i}, \qquad \mathbf{B}_{\phi_e,\phi_e} = \mathbf{K}_{\boldsymbol{\sigma}_e+\boldsymbol{\sigma}_i}.$$

The third block row is the formulation of the harmonic body potential $\phi_b$ and the matrix $\mathbf{C}_{\phi_b,\phi_b}$ equals the system matrix $\mathbf{K}_{\boldsymbol{\sigma}_b}$ in Eq. (1.65). The coupling condition on the flux $q$ in Eq. (1.18b) is accounted for by including the boundary matrix $\mathbf{B}_{\Gamma_M}$ in the last column. The minus sign comes from the fact that the outward normal vector on $\Gamma_M$ as the boundary of $\Omega_B$ is has the opposite direction to the normal vector on $\Gamma_M$ that is used for the models in the muscle domain $\Omega_M$. Using the helper variable $\mathbf{q}^{(i+1)}$, the second and third row of Eq. (1.66) are coupled according to the prescribed condition in Eq. (1.18b).

The other coupling condition, Eq. (1.18a), is accounted for by the last block row in Eq. (1.65). The degrees of freedom for the extracellular potential $\boldsymbol{\phi}^{(i+1)}_e$ and the body potential $\boldsymbol{\phi}^{(i+1)}_b$ have equal values on the boundary $\Gamma_M$. The matrices $\mathbf{I}_{\Gamma_M,\phi_e}$ and $\mathbf{I}_{\Gamma_M,\phi_b}$ are identity matrices that only have nonzero entries on the diagonal for the boundary degrees of freedom in the meshes of muscle domain and body domain, respectively.

Because the vector $\mathbf{q}^{(i+1)}$ is not an unknown in the system, the respective values in Eq. (1.66) have to be eliminated. As a result, we obtain the following system, which is

formulated for a generic number $N_{\mathrm{MU}}$ of MUs:

$$\left[\begin{array}{ccc|c|c} \mathbf{A}^{1}_{V_m,V_m} & & & \mathbf{B}^{1}_{V_m,\phi_e} & \\ & \ddots & & \vdots & \\ & & \mathbf{A}^{N_{\mathrm{MU}}}_{\phi_e,V_m} & \mathbf{B}^{N_{\mathrm{MU}}}_{V_m,\phi_e} & \\ \mathbf{B}^{1}_{\phi_e,V_m} & \cdots & \mathbf{B}^{N_{\mathrm{MU}}}_{\phi_e,V_m} & \mathbf{B}_{\phi_e,\phi_e} & \mathbf{D} \\ \hline & & & \mathbf{E} & \tilde{\mathbf{C}}_{\phi_b,\phi_b} \end{array}\right] \left[\begin{array}{c} \mathbf{V}^{1,(i+1)}_{m} \\ \vdots \\ \mathbf{V}^{N_{\mathrm{MU}},(i+1)}_{m} \\ \hline \boldsymbol{\phi}^{(i+1)}_{e} \\ \hline \tilde{\boldsymbol{\phi}}^{(i+1)}_{b} \end{array}\right] = \left[\begin{array}{c} \mathbf{b}^{1,(i)}_{V_m} \\ \vdots \\ \mathbf{b}^{N_{\mathrm{MU}},(i)}_{V_m} \\ \mathbf{0} \\ \hline \mathbf{0} \end{array}\right]. \tag{1.67}$$

Formally, the elimination step is carried out by adding the equations of the third block row in Eq. (1.66), that correspond to the boundary degrees of freedom on $\Gamma_M$, to the corresponding equations of the same degreres of freedom in the second block row. This eliminates the last block column, which corresponds to $\mathbf{q}^{(i+1)}$. Next, the duplicate boundary degrees of freedom, that appear in both the $\Omega_M$ and $\Omega_B$ meshes, get unified. The corresponding matrix columns in the third block column are removed. To preserve the entries in the third block row, they are added in the sub matrix of block row three and block column two.

Now considering the updated matrix equation in Eq. (1.67), all sub blocks are equal to Eq. (1.66), except for the former matrix $\mathbf{C}_{\phi_b,\phi_b}$ and the new matrices $\mathbf{D}$ and $\mathbf{E}$. The new matrix $\tilde{\mathbf{C}}_{\phi_b,\phi_b}$ is obtained from $\mathbf{C}_{\phi_b,\phi_b}$ by removing all rows and columns of boundary degrees of freedom. The removed entries are contained in the new matrices $\mathbf{D}$ and $\mathbf{E}$.

The size of the system matrix in Eq. (1.67) equals $a \times a$, where the number $a$ is composed of $N_{\mathrm{MU}} + 1$ times the number of degrees of freedom in the muscle mesh plus the number of degrees of freedom in the fat layer mesh without the boundary degrees of freedom on $\Gamma_M$. Accordingly, the vector $\tilde{\boldsymbol{\phi}}^{(i+1)}_b$ is the same as $\boldsymbol{\phi}^{(i+1)}_b$ except that it does not contain the boundary degrees of freedom, which are already included in $\boldsymbol{\phi}^{(i+1)}_e$.

Equation (1.67) describes one iteration of the Crank-Nicolson scheme that is used to solve the multidomain model. This iteration is carried out alternatingly with the subcellular model according to the chosen operator splitting scheme.

The first $N_{\mathrm{MU}}$ block rows in Eq. (1.67) contain the second multidomain equation for every MU. The second-to-last block row contains the first multidomain equation and the last block row contains the body fat layer model.

Because of the implicit formulation, electric conduction in the intracellular and extracellular space and the body domain are bidirectionlly coupled. Therefore, the model can

be used to simulate the effects of natural activation in the muscle on EMG signals on the skin surface as well as the reverse effect of external stimulation on the surface on the electrophysiology.

### 1.3.6 Discretization of the Fiber Based Electrophysiology Model

The fiber based electrophysiology model consists of multiple independent 1D fiber domains, where the monodomain equation Eq. (1.11) is solved. The transmembrane voltage $V_m$ is then mapped to a 3D mesh of the muscle domain and unidirectionally coupled to the first bidomain equation Eq. (1.9a). The first bidomain equation is solved for the extracellular potential $\phi_e$ and possibly the electric potential $\phi_b$ in the body fat domain, which corresponds to EMG signals on the skin surface.

The temporal discretization of the monodomain equation was described in Sec. 1.3.1. The diffusion term within the operator splitting requires a spatial discretization for which we use the Finite Element Method. This 1D diffusion equation is given as

$$\frac{\partial V_m}{\partial t} = \frac{\sigma_{\text{eff}}}{A_m C_m} \frac{\partial^2 V_m}{\partial x^2}. \tag{1.68}$$

It can be solved using a timestepping scheme such as the implicit Euler method to obtain time-discrete values $V_m^{(i)}, i = 1, 2, \ldots$ for the transmembrane potential. The discretization leads to the matrix equation given in Eq. (1.48) and to the variants presented in Sec. 1.3.3 if mass lumping is used. In the stiffness and mass matrices, the anisotropic conduction tensor is replaced by the constant scalar prefactor $c := \sigma_{\text{eff}}/(A_m C_m)$ of the spatial second derivative in Eq. (1.68).

The first bidomain equation Eq. (1.9a) is a 3D Poisson problem in terms of the unknown extracellular potential $\phi_e$. According to Eq. (1.51), the Finite Element discretization is given by

$$\mathbf{K}_{\sigma_i+\sigma_e} \boldsymbol{\phi}_e^{(i+1)} = -\mathbf{B}_{\Gamma_f} \mathbf{f} + \mathbf{rhs},$$

where the right hand side **rhs** of the Poisson problem is given by

$$\mathbf{rhs} = -\mathbf{K}_{\sigma_i} \mathbf{V}_{m,3D}^{(i+1)}.$$

Here, $\boldsymbol{\phi}_e^{(i+1)}$ and $\mathbf{V}_{m,3D}^{(i+1)}$ are the vectors of degrees of freedom on the 3D mesh for the extracellular potential $\phi_e$ and the membrane potential $V_m$ at timestep $(i+1)$. With the

homogeneous Neumann boundary conditions for $V_m$ and $\phi_e$ given in Eq. (1.12), the boundary term $\mathbf{B}_{\Gamma_f}$ vanishes.

In summary, the following matrix equations are solved for the fiber based electrophysiology model with $n$ fibers:

$$\begin{bmatrix} \mathbf{A} & & \\ & \ddots & \\ & & \mathbf{A} \end{bmatrix} \begin{bmatrix} \mathbf{V}_m^{1,(i+1)} \\ \vdots \\ \mathbf{V}_m^{n,(i+1)} \end{bmatrix} = \begin{bmatrix} \mathbf{V}_m^{1,(i)} \\ \vdots \\ \mathbf{V}_m^{n,(i)} \end{bmatrix}, \tag{1.69a}$$

$$\mathbf{V}_{m,3D}^{(i+1)} = \mathbf{P} \begin{bmatrix} \mathbf{V}_m^{1,(i+1)} \\ \vdots \\ \mathbf{V}_m^{n,(i+1)} \end{bmatrix}, \tag{1.69b}$$

$$\mathbf{K}_{\boldsymbol{\sigma}_i+\boldsymbol{\sigma}_e} \boldsymbol{\phi}_e^{(i+1)} = -\mathbf{M}_{\boldsymbol{\sigma}_i} \mathbf{V}_{m,3D}^{(i+1)} \tag{1.69c}$$

with the system matrix $\mathbf{A}$ for a single fiber given according to Eq. (1.53b) by

$$\mathbf{A} = \mathbf{I} - dt\, \mathbf{M}_c^{-1} \mathbf{K}_c.$$

Equation (1.69a) solves the diffusion part of the operator splitting in Eq. (1.42). After the values $\mathbf{V}_m^{j,(i+1)}$ for the timestep $(i+1)$ are computed on the 1D fiber meshes, the homogenized vector $\mathbf{V}_{m,3D}^{(i+1)}$ in the 3D mesh of the muscle domain $\Omega_M$ is obtained by the prolongation operation $\mathbf{P}$ in Eq. (1.69b). The homogenized vector is used in the right hand side of the bidomain model in Eq. (1.69c), which computes the discretized extracellular potential $\boldsymbol{\phi}_e^{(i+1)}$.

Equation (1.69c) can be extended by adding a body fat layer $\Omega_B$ and the corresponding model for the electric potential $\phi_b^{(i+1)}$. Then, the vector of unknowns contains the degrees of freedom for both $\phi_e^{(i+1)}$ and $\phi_b^{(i+1)}$. The stiffness matrix $\mathbf{K}_{\boldsymbol{\sigma}_i+\boldsymbol{\sigma}_e}$ is obtained by integrating over both meshes in $\Omega_M \cup \Omega_B$. Only in the elements of the Finite Element mesh for $\Omega_B$, the conduction tensors are redefined as $\boldsymbol{\sigma}_i = \mathbf{0}$ and $\boldsymbol{\sigma}_e = \boldsymbol{\sigma}_b$. This sets the right hand side of Eq. (1.69c) to zero in $\Omega_B$ and the solution $\phi_b$ in harmonic according to the model in Eq. (1.17). The coupling conditions Eq. (1.18) between $\phi_e$ and $\phi_b$ and the outer Neumann boundary conditions Eq. (1.19) for $\phi_b$ are satisfied automatically by this approach.

The comparison between the discretized multidomain model in Eq. (1.67) with the discretized fiber based model in Eq. (1.69) reveals several differences. Whereas the multidomain description consists of a single coupled linear system for electric conduction

in the intracellular, extracellular and body domains, the formulations are only unidirectionally coupled in the fiber based description. While the multidomain model always computes the EMG signals on the skin surface in every timestep, the corresponding model in the fiber based description can be solved with larger timestep widths, using subcycling for the action potential propagation model.

As can be seen in Eq. (1.69a), the system matrix is decoupled and contains independent problems for every fiber. This is an advantage compared to the multidomain model, where a system describing the whole muscle domain has to be solved. On the downside, separate representations of the transmembrane voltage $V_m$ exist in the fiber based description. The representation in the 3D mesh has to be computed by interpolation from the representation on the fibers. The multidomain description has a single vector of degrees of freedom for $V_m$ with less entries than in the fiber-based description.

### 1.3.7 Summary of Domains and Meshes

Various Finite Element meshes occur in the formulation of the multi-scale model. If the fiber based description is used, the description requires Finite Element meshes for the 1D fiber domains $\Omega_f^j$ for $j = 1, \ldots, n$. Further meshes are needed for the 3D muscle domain $\Omega_M$ and for the 3D body domain $\Omega_B$. The meshes for $\Omega_M$ and $\Omega_B$ share nodes on their common boundary $\Gamma_M$. The fiber meshes are embedded in the muscle domain. Their nodes do not necessarily have to coincide with the nodes of the muscle mesh.

The subcellular model is solved at locations $\Omega_s^i$ for $i = 1, \ldots, m$. These locations are the nodes of the fiber meshes for the fiber based description and the nodes of the muscle mesh for the multidomain description. We therefore have the inclusion $\Omega_s^i \subset \Omega_f^j \subset \Omega_M$.

For the solid mechanics model, the unified 3D domain $\Omega = \Omega_M \cup \Omega_B$ is used. The mesh for the continuum mechanics formulation can be different from the meshes used for the electrophysiology model. In fact, the continuum mechanics mesh has special requirements in order to yield a consistent formulation. Our implementation uses two overlayed meshes of quadratic and linear hexahedral elements for displacements and the hydrostatic pressure.

Often, the required accuracy of the electrophysiology model is higher than for the continuum mechanics model, such that differently resolved meshes can be used. To facilitate data mapping, the nodes of the mechanics mesh should be chosen as subset of the nodes of the electrophysiology meshes.

## 1.4 Discretization and Solution Approach for the Solid Mechanics Model

After the formulation of linear and nonlinear models for solid mechanics in Sec. 1.2, this section discusses their discretization and derives Finite Element formulations for the linearized model and the nonlinear model, both static and dynamic. We also describe the algorithms used to obtain a numeric solution.

The implementation of a solver for generic hyperelastic descriptions is an interdisciplinary endeavour, if parallel execution is exploited and the model is integrated in a multi-scale biomechanics model. Therefore, we give a comprehensive derivation of the formulas used to numerically solve the equations matching the implementation in OpenDiHu, such that the implementation is also comprehensible for readers that are not specialized in the field of continuum mechanics. More details on Finite Element discretizations for solid mechanics models can be found in the literature [Zie77]; [Sus87]; [Zie05].

### 1.4.1 Discretization of the Linear Model

In this section, we discuss the linearized and static model. Besides the nonlinear model, our software OpenDiHu also implements the linearized description. The linear model exhibits better numerical properties and can be solved faster than the generic model. Thus, it can serve as a toy problem or can be used for mechanical systems, where the linearization assumptions are valid.

By assuming small strains, we can use the linearized kinematic relation in Eq. (1.25) to express the linear strain tensor $\boldsymbol{\varepsilon}$. The material model is Hooke's law formulated in Eq. (1.33). It relates the strain to the Cauchy stress by $\boldsymbol{\sigma} = \mathbb{C} : \boldsymbol{\varepsilon}$.

Using variational calculus, the system response of external forces and infinitesimal, compatible, virtual displacements $\delta\mathbf{u}$ is studied. We start with the *principle of virtual work*, which states that in equilibrium the virtual work $\delta W$ performed by external forces along any virtual displacements $\delta\mathbf{u}$ is zero. Equivalently, the external virtual work $\delta W_{\text{ext}}$ is equal to the internal virtual work $\delta W_{\text{int}}$:

$$\delta W_{\text{int}}(\mathbf{u}, \delta\mathbf{u}) = \delta W_{\text{ext}}(\delta\mathbf{u}) \qquad \forall \delta\mathbf{u} \in H_0^1(\Omega). \tag{1.70}$$

Here, the external virtual work $\delta W_{\text{ext}}$ is given by the product of external forces $\mathbf{t}$ and the virtual displacements $\delta\mathbf{u}$ at the same location. The internal virtual work $\delta W_{\text{int}}$ is the body's response in terms of stresses $\boldsymbol{\sigma}$ and virtual strains $\boldsymbol{\varepsilon}$. In summary, Eq. (1.70) is equivalent to the following equilibrium equation:

$$\int_\Omega \boldsymbol{\sigma}(\mathbf{u}) : \delta\boldsymbol{\varepsilon}\,\mathrm{d}\mathbf{x} = \int_{\partial\Omega} \mathbf{t} : \delta\mathbf{u}\,\mathrm{d}\mathbf{x} \qquad \forall \delta\mathbf{u} \in H_0^1(\Omega). \tag{1.71}$$

The vectors contain the degrees of freedom of a Finite Element discretization. The operator ":" denotes the component-wise product.

Often, it is easier to write the equations in component form. Indices $a, b, c, \ldots$ are used to specify a dimension index in $\{1, \ldots, d\}$. The letters $L, M \in \{1, \ldots, N\}$ denote indices over degrees of freedom in a mesh with $N$ nodes. The Einstein sum convention is used where repeated indices implicitly indicate summation, except when the indices are in parantheses. Thus, the right hand side $\mathbf{f}$ of Eq. (1.71) with ansatz functions $\phi^L$ and the degrees of freedom $\delta u_a^L$ of $\delta\mathbf{u}$ can be written as:

$$\mathbf{f}_a = \int_{\partial\Omega} t_{(a)}\, \delta u^L_{(a)}\, \phi^L\,\mathrm{d}\mathbf{x}.$$

By combining the kinematic relation between displacements $\mathbf{u}$ and linearized strains $\boldsymbol{\varepsilon}$ in Eq. (1.25), the material relation between $\boldsymbol{\varepsilon}$ and the stress $\boldsymbol{\sigma}$ in Eq. (1.33), the equilibrium relation between $\boldsymbol{\sigma}$ and the right hand side vector $\mathbf{f}$ in Eq. (1.71) and after discretizing displacements and virtual displacements, we get the following linear matrix equation:

$$\mathbf{K}\mathbf{u} = \mathbf{f}. \tag{1.72}$$

The stiffness matrix $\mathbf{K}$ has rows and columns for every combination of degree of freedom $L, M \in \{1, \ldots, N\}$ and dimension indices $a, b \in \{1, 2, 3\}$. The entries are given by:

$$\mathbf{K}_{LaMb} = \int_\Omega \mathbb{C}_{adbc} \frac{\partial\phi^L(\mathbf{x})}{\partial x_d} \frac{\partial\phi^M(\mathbf{x})}{\partial x_c}\,\mathrm{d}\mathbf{x}.$$

The resulting model in Eq. (1.72) describes the passive behavior of a body under the linearization assumptions and can be used in an appropriate biomechanical application.

However, for contracting muscle tissue, we also need to incorporate active stresses that are generated at the sarcomeres in the muscle. As described in Eq. (1.35), an active stress term $\boldsymbol{\sigma}^{\text{active}}$ can be considered. Because this active term is prescribed by the activation

dynamics and the subcellular model, it has to appear on the right hand side of the linear model. We add the active stress term $\boldsymbol{\sigma}^{\text{active}}$ to the external virtual work in Eq. (1.70), yielding the equation:

$$\delta W_{\text{int}}(\mathbf{u}, \delta\mathbf{u}) = \mathbf{f} + \int_\Omega \boldsymbol{\sigma}^{\text{active}} : \delta\boldsymbol{\varepsilon}\_ \, \mathrm{d}\mathbf{x} \qquad \forall \delta\mathbf{u} \in H^1_0(\Omega). \tag{1.73}$$

The active stress is associated with compression, i.e., negative virtual strains $\delta\boldsymbol{\varepsilon} < 0$. Therefore, we use $\delta\boldsymbol{\varepsilon}\_$ which is defined equal to $\delta\boldsymbol{\varepsilon}$ for $\delta\boldsymbol{\varepsilon} < 0$ and zero otherwise. From Eq. (1.73), we get the same discretized linear system as in Eq. (1.72), but with an additional term $\mathbf{f}^{\text{active}}$ in the right hand side that contains the discretized prescribed active stress field $\boldsymbol{\sigma}^{\text{active}}_{ab}(\mathbf{x})$:

$$\mathbf{f}^{\text{active}}_{La} = \int_\Omega \boldsymbol{\sigma}^{\text{active}}_{ab}(\mathbf{x}) \frac{\partial \phi^L(\mathbf{x})}{\partial x_b} \, \mathrm{d}\mathbf{x}.$$

## 1.4.2 Discretization of the Nonlinear Static Hyperelastic Model

Next, we discuss the discretization of the nonlinear solid mechanics model, which uses the model equations introduced in Sec. 1.2. We begin with the discretization of a static, incompressible problem, where no velocities have to be considered. The discretization is extended to the dynamic model in Sec. 1.4.6.

As described in Sec. 1.2.4, the equilibrium equation can be formulated in terms of the *Hellinger-Reissner energy functional* $\Pi_L(\mathbf{u}, p) = \Pi_{\text{int}}(\mathbf{u}, p) + \Pi_{\text{ext}}(\mathbf{u})$ given in Eq. (1.31). It consists of the external energy functional, given in Eq. (1.32) as

$$\Pi_{\text{ext}}(\mathbf{u}) = -\int_{\Omega_0} \mathbf{B}\,\mathbf{u} \, \mathrm{d}V - \int_{\partial\Omega_0^t} \bar{\mathbf{T}}\,\mathbf{u} \, \mathrm{d}S,$$

with body force $\mathbf{B}$ and surface traction $\bar{\mathbf{T}}$, and of the internal energy functional

$$\Pi_{\text{int}}(\mathbf{u}, p) = \int_{\Omega_0} \Psi_{\text{iso}}\big(\bar{\mathbf{C}}(\mathbf{u})\big) \, \mathrm{d}V + \int_{\Omega_0} p\,\big(J(\mathbf{u}) - 1\big) \, \mathrm{d}V. \tag{1.74}$$

Here, $\Psi_{\text{iso}}$ is the isochoric strain-energy density function introduced in Eq. (1.38) in terms of the reduced right Cauchy-Green tensor $\bar{\mathbf{C}}$ defined in Eq. (1.37). The first term in Eq. (1.74) describes the isochoric elastic response of the material, the second term adds the incompressibility constraint $J = 1$ with the Lagrange multiplier $p$. The value of $p$ is computed as part of the model and can be identified as the hydrostatic pressure.

Therefore, the second term is interpreted as the elastic response to compression and is included in the internal energy functional $\Pi_{\text{int}}$.

According to the *principle of stationary potential energy*, the system is in equilibrium, if the potential energy functional is stationary. This is the case, if the first variation $\delta\Pi_L$ is zero. Using the additive structure of $\Pi_L$, we can express the principle of stationarity as

$$D_{\delta\mathbf{u}}\Pi_L(\mathbf{u},p) = D_{\delta\mathbf{u}}\Pi_{\text{int}}(\mathbf{u},p) + D_{\delta\mathbf{u}}\Pi_{\text{ext}}(\mathbf{u}) \overset{!}{=} 0, \qquad \forall\delta\mathbf{u} \tag{1.75a}$$

$$D_{\delta p}\Pi_L(\mathbf{u},p) = D_{\delta p}\Pi_{\text{int}}(\mathbf{u},p) \overset{!}{=} 0 \qquad \forall\delta p. \tag{1.75b}$$

The variations of the internal and external energy functionals are defined as

$$D_{\delta\mathbf{u}}\Pi(\mathbf{u}) = \frac{\mathrm{d}}{\mathrm{d}\varepsilon}\,\Pi(\mathbf{u}+\varepsilon\delta\mathbf{u})\Big|_{\varepsilon=0}, \qquad D_{\delta p}\Pi(p) = \frac{\mathrm{d}}{\mathrm{d}\varepsilon}\,\Pi(p+\varepsilon\delta p)\Big|_{\varepsilon=0}. \tag{1.76}$$

They can be identified as the internal and external virtual work,

$$D_{\delta\mathbf{u}}\Pi_{\text{int}}(\mathbf{u},p) = \delta W_{\text{int}}, \qquad D_{\delta\mathbf{u}}\Pi_{\text{ext}}(\mathbf{u}) = -\delta W_{\text{ext}}.$$

Thus, Eq. (1.75a) can be expressed as

$$\delta W_{\text{int}} - \delta W_{\text{ext}} = 0,$$

which is the form of the equilibrium equation that was used in Eq. (1.70) in the derivation of the linearized model in Sec. 1.4.1 . The Euler-Lagrange equations corresponding to the variational problem are the local incompressibility constraint and the partial differential equation of balance of momentum presented in Eqs. (1.41a) and (1.41b).

Executing the derivative in the definitions of the variations in Eq. (1.76) yields the following terms:

$$D_{\delta\mathbf{u}}\Pi_{\text{int}}(\mathbf{u},p) = \int_{\Omega_0} \mathbf{S}(\mathbf{u},p) : \delta\mathbf{E}(\delta\mathbf{u})\,\mathrm{d}V, \qquad D_{\delta p}\Pi_{\text{int}}(\mathbf{u},p) = \int_{\Omega_0} \big(J(\mathbf{u})-1\big)\delta p\,\mathrm{d}V,$$

$$D_{\delta\mathbf{u}}\Pi_{\text{ext}}(\mathbf{u}) = -\int_{\Omega_0} \mathbf{B}\cdot\delta\mathbf{u}\,\mathrm{d}V - \int_{\partial\Omega_0^t} \bar{\mathbf{T}}\cdot\delta\mathbf{u}\,\mathrm{d}S,$$

where the variational variables $\delta p, \delta\mathbf{u}$ and $\delta\mathbf{E}$ are the virtual pressure, virtual displacements, and virtual strains.

We discretize the solutions of the functional for the displacements $\mathbf{u}(\mathbf{x})$ and pressure

$p(\mathbf{x})$ and their variations using different ansatz functions $\phi^L$, $L = 1,\dots,N_u$ and $\psi^L$, $L = 1,\dots,N_p$:

$$u_a = \hat{u}_a^L \phi_{(a)}^L, \qquad \delta u_a = \delta\hat{u}_a^L \phi_{(a)}^L, \qquad p = \hat{p}^L \psi^L, \qquad \delta p = \delta\hat{p}^L \psi^L.$$

Again, Einstein summation over repeated indices, in this case the index $L$, is used. The displacements function is vector-valued and given by $\mathbf{u}(\mathbf{x}) = (u_1(\mathbf{x}), u_2(\mathbf{x}), u_3(\mathbf{x}))^\top$. The vectors containing the degrees of freedom are denoted by $\hat{\mathbf{u}} = (\hat{u}^L)_{L=1,\dots,N_u}$ and $\hat{\mathbf{p}} = (\hat{p}^L)_{L=1,\dots,N_p}$.

The kinematics equation to compute virtual strains from virtual displacements follows from Eq. (1.24) in Lagrangian description and is given by $\delta\mathbf{E} = \operatorname{sym}(\mathbf{F}^\top \nabla \mathbf{u})$. Its discretized form is given as follows, where the subscript comma $\square_{,A}$ indicates the derivative with respect to the indexed coordinate $\mathbf{X}_A$:

$$\delta E_{AB} = \frac{1}{2}\left(F_{aB}\,\phi_{(a),A}^M + F_{aA}\,\phi_{(a),B}^M\right)\delta\hat{u}_a^M.$$

In summary, the resulting set of discretized nonlinear equations can be formulated as:

$$\delta W_{\text{int}}(\mathbf{u}, p) - \delta W_{\text{ext}} = 0 \qquad \forall\, \delta\mathbf{u}, \tag{1.77}$$

$$D_{\delta p}\Pi_L(\mathbf{u}) = 0 \qquad \forall\, \delta p, \tag{1.78}$$

with the following discretized terms:

$$\delta W_{\text{int}}(\hat{\mathbf{u}}, \hat{\mathbf{p}}) = \int_\Omega \frac{1}{2} S_{AB}(\hat{\mathbf{u}}, \hat{\mathbf{p}})\left(F_{aB}\,\phi_{(a),A}^M + F_{aA}\,\phi_{(a),B}^M\right)\delta\hat{u}_a^M \,\mathrm{d}V, \tag{1.79a}$$

$$\delta W_{\text{ext}} = \int_\Omega B_a \phi_{(a)}^M\,\delta\hat{u}_a^M \,\mathrm{d}V + \int_{\partial\Omega} \bar{T}_a^L\,\phi_{(a)}^L\,\phi_{(a)}^M\,\delta\hat{u}_a^M \,\mathrm{d}S, \tag{1.79b}$$

$$D_{\delta p}\Pi_L(\hat{\mathbf{u}}) = \int_\Omega \big(J(\hat{\mathbf{u}}) - 1\big)\,\delta p \,\mathrm{d}V. \tag{1.79c}$$

The nonlinear system of equations in Eqs. (1.77) and (1.79) can now be solved for the unknown vectors $\hat{\mathbf{u}}$ and $\hat{\mathbf{p}}$ of degrees of freedom using a Newton scheme.

### 1.4.3 Discretization of the Nonlinear Dynamic Hyperelastic Model

We extend the discretization of the static model in the last section for the dynamic model. The vector of unknowns is extended by a velocity function $\mathbf{v} : \Omega_t \to \mathbb{R}^3$. The additional equation $\dot{\mathbf{u}} = \mathbf{v}$ relates the displacements and the velocity.

As noted in the derivation of the equilibrium equation in Sec. 1.2.4, the body force term $\mathbf{B}$ in the external energy functional also includes the inertial forces $\mathbf{B}_{\text{inertial}} = \rho_0 \dot{\mathbf{v}}$ to describe the dynamic behavior.

The resulting nonlinear system of equations is given as follows:

$$\delta W_{\text{int}}(\mathbf{u}, p) - \delta W_{\text{ext}}(\mathbf{v}) = 0 \qquad \forall\, \delta\mathbf{u}, \tag{1.80a}$$

$$\mathbf{v} = \dot{\mathbf{u}}, \tag{1.80b}$$

$$D_{\delta p}\Pi_L(\mathbf{u}) = 0 \qquad \forall\, \delta p. \tag{1.80c}$$

### 1.4.4 Computation of the Stress Tensor and the Elasticity Tensor

In the Newton solver, we need to compute the stress tensor $\mathbf{S}$ and its derivative $\mathbb{C}$, called the elasticity tensor, given the current displacement field $\mathbf{u}$. The relations are defined by the material model given by the strain energy function. This sections presents the algorithm how to obtain the values of $\mathbf{S}$ and $\mathbb{C}$ from the displacements $\mathbf{u}$. While the derivation is formulated in terms of the displacement function $\mathbf{u}$, it is also valid for the Finite Element discretization, i.e., using the vector $\hat{\mathbf{u}}$ of degrees of freedom instead.

Following Eq. (1.36), the second Piola-Kirchhoff stress $\mathbf{S}$ is given by a the derivative of the strain energy function $\Psi$ with respect to $\mathbf{C}$. For the representation using the invariants, the chain rule has to be used:

$$\mathbf{S} = 2\frac{\partial \Psi(\mathbf{C})}{\partial \mathbf{C}} = \frac{\partial \Psi}{\partial I_a}\frac{\partial I_a}{\partial \mathbf{C}}.$$

Using the decoupled form, the resulting stresses are also decoupled as $\mathbf{S} = \mathbf{S}_{\text{vol}} + \mathbf{S}_{\text{iso}}$. The volumetric stress $\mathbf{S}_{\text{vol}}$ describes the elastic response to compression, the isochoric stress $\mathbf{S}_{\text{iso}}$ describes the response to the deviatoric deformation. In the following, all steps to compute these stresses are listed. The rationale is to give a condensed reference of the

implemented algorithm in OpenDiHu to facilitate further development. For the derivation of all intermediate steps, we refer to the literature [Hol00].

At first, the reduced stress tensor $\bar{\mathbf{S}}$ that neglects the volumetric change is formulated as:

$$\bar{\mathbf{S}} = 2\frac{\partial \Psi_{\text{iso}}(\bar{I}_1, \bar{I}_2, \bar{I}_4, \bar{I}_5)}{\partial \bar{\mathbf{C}}} = \bar{\gamma}_1 \mathbf{I} + \bar{\gamma}_2 \bar{\mathbf{C}} + \bar{\gamma}_4 \mathbf{a}_0 \otimes \mathbf{a}_0 + \bar{\gamma}_5 (\mathbf{a}_0 \otimes \bar{\mathbf{C}} \mathbf{a}_0 + \mathbf{a}_0 \bar{\mathbf{C}} \otimes \mathbf{a}_0).$$

In case of an isotropic material, the terms involving $\mathbf{a}_0$ are not needed. The prefactors are given by derivatives of the strain energy function with respect to the reduced invariants:

$$\bar{\gamma}_1 = 2\left(\frac{\partial \Psi_{\text{iso}}(\bar{I}_1, \bar{I}_2)}{\partial \bar{I}_1} + \bar{I}_1 \frac{\partial \Psi_{\text{iso}}(\bar{I}_1, \bar{I}_2)}{\partial \bar{I}_2}\right), \quad \bar{\gamma}_2 = -2\frac{\partial \Psi_{\text{iso}}(\bar{I}_1, \bar{I}_2)}{\partial \bar{I}_2}, \quad \bar{\gamma}_4 = 2\frac{\partial \Psi_{\text{iso}}}{\partial \bar{I}_4}$$

$$\bar{\gamma}_5 = 2\frac{\partial \Psi_{\text{iso}}}{\partial \bar{I}_5}$$

Using the fourth order identity tensor $\mathbb{I}$ and the projection tensor $\mathbb{P}$,

$$(\mathbb{I})_{abcd} = \delta_{ac}\,\delta_{bd}, \qquad \mathbb{P} = \mathbb{I} - \frac{1}{3}\mathbf{C}^{-1} \otimes \mathbf{C},$$

the stress tensors can finally be computed as

$$\mathbf{S}_{\text{iso}} = J^{-2/3}\mathbb{P} : \bar{\mathbf{S}}, \qquad \mathbf{S}_{\text{vol}} = J\,p\,\mathbf{C}^{-1}, \qquad \mathbf{S} = \mathbf{S}_{\text{iso}} + \mathbf{S}_{\text{vol}}.$$

In the compressible case including the penalty method, the value of $p$, that is needed for $\mathbf{S}_{\text{vol}}$, is given by the constitutive model as $p = \mathrm{d}\Psi_{\text{vol}}(J)/\mathrm{d}J$. In the incompressible case, $p$ is the unknown Lagrange multiplier that gets computed as part of the numerical solution. In that case, $p$ has the physical meaning of the hydrostatic pressure.

Using the present algorithm, the stress tensor $\mathbf{S}$ can, thus, be computed from derivatives of the strain energy function $\Psi$ and the right Cauchy Green tensor $\mathbf{C}$, which can be calculated from the displacement field $\mathbf{u}$.

Another important quantity for the numerical solution of the nonlinear system is the fourth order elasticity tensor $\mathbb{C}$, which is defined as

$$\mathbb{C} = 2\frac{\partial \mathbf{S}(\mathbf{C})}{\partial \mathbf{C}} = 4\frac{\partial^2 \Psi(\mathbf{C})}{\partial \mathbf{C} \partial \mathbf{C}}.$$

It is the derivative of the stress tensor and is required in the Jacobian matrix of an iteration of the nonlinear Newton solver. Like the material tensor in Eq. (1.34), it shows major

and minor symmetries and has 21 independent entries.

Like the stress tensor, the elasticity tensor is also additively composed into a volumetric term $\mathbb{C}_{\text{vol}}$ and an isochoric term $\mathbb{C}_{\text{iso}}$. The volumetric term can be computed by:

$$\mathbb{C}_{\text{vol}} = J\,\tilde{p}\,\mathbf{C}^{-1}\otimes\mathbf{C}^{-1} - 2J\,p\,\mathbf{C}^{-1}\odot\mathbf{C}^{-1},\quad \left(\mathbf{C}^{-1}\odot\mathbf{C}^{-1}\right)_{abcd} = \frac{1}{2}\left(C^{-1}_{ac}\,C^{-1}_{bd} + C^{-1}_{ad}\,C^{-1}_{bc}\right).$$

The term includes two pressure variables $\tilde{p}$ and $p$. In the incompressible formulation, both variables equals the Lagrange multiplier $p$. For the compressible formulation, $\tilde{p}$ is derived as $\tilde{p} = p + J\,\mathrm{d}p/\mathrm{d}J$ and $p$ is computed from the volumetric strain energy function as stated above.

The isochoric term $\mathbb{C}_{\text{iso}}$ of the elasticity tensor follows from the following algorithm listing the quantities to compute:

$$\bar{\delta}_1 = 4\left(\frac{\partial^2\Psi_{\text{iso}}}{\partial\bar{I}_1\,\partial\bar{I}_1} + 2\,\bar{I}_1\frac{\partial^2\Psi_{\text{iso}}}{\partial\bar{I}_1\,\partial\bar{I}_2} + \frac{\partial\Psi_{\text{iso}}}{\partial\bar{I}_2} + \bar{I}_1^2\,\frac{\partial^2\Psi_{\text{iso}}}{\partial\bar{I}_2\,\partial\bar{I}_2}\right),\ \bar{\delta}_2 = -4\left(\frac{\partial^2\Psi_{\text{iso}}}{\partial\bar{I}_1\,\partial\bar{I}_2} + \bar{I}_1\,\frac{\partial^2\Psi_{\text{iso}}}{\partial\bar{I}_2\,\partial\bar{I}_2}\right),$$

$$\bar{\delta}_3 = 4\frac{\partial^2\Psi_{\text{iso}}}{\partial\bar{I}_2\,\partial\bar{I}_2},\quad \bar{\delta}_4 = -4\frac{\partial\Psi_{\text{iso}}}{\partial\bar{I}_2},\quad \bar{\delta}_5 = 4\left(\frac{\partial^2\Psi_{\text{iso}}}{\partial\bar{I}_1\,\partial\bar{I}_4} + \bar{I}_1\frac{\partial^2\Psi_{\text{iso}}}{\partial\bar{I}_2\,\partial\bar{I}_4}\right),$$

$$\bar{\delta}_6 = -4\frac{\partial^2\Psi_{\text{iso}}}{\partial\bar{I}_2\,\partial\bar{I}_4},\ \bar{\delta}_7 = 4\frac{\partial^2\Psi_{\text{iso}}}{\partial\bar{I}_4\,\partial\bar{I}_4},\ \mathbb{I}_{abcd} = \delta_{ac}\,\delta_{bd},\ \bar{\mathbb{I}}_{abcd} = \delta_{ad}\,\delta_{bc},\ \mathbb{S} = (\mathbb{I}+\bar{\mathbb{I}})/2,$$

$$\frac{\partial\bar{I}_5}{\partial\bar{\mathbf{C}}} = \mathbf{a}_0\otimes\bar{\mathbf{C}}\,\mathbf{a}_0 + \mathbf{a}_0\,\bar{\mathbf{C}}\otimes\mathbf{a}_0,\quad \frac{\partial^2\bar{I}_5}{\partial\bar{\mathbf{C}}\partial\bar{\mathbf{C}}} = \frac{\partial}{\partial\bar{\mathbf{C}}}\left(\mathbf{a}_0\otimes\bar{\mathbf{C}}\,\mathbf{a}_0 + \mathbf{a}_0\,\bar{\mathbf{C}}\otimes\mathbf{a}_0\right),$$

$$\bar{\mathbb{C}} = J^{-4/3}\Big( \bar{\delta}_1 \mathbf{I}\otimes\mathbf{I} + \bar{\delta}_2 \left(\mathbf{I}\otimes\bar{\mathbf{C}} + \bar{\mathbf{C}}\otimes\mathbf{I}\right) + \bar{\delta}_3 \bar{\mathbf{C}}\otimes\bar{\mathbf{C}} + \bar{\delta}_4 \mathbb{S} + \bar{\delta}_5 \left(\mathbf{I}\otimes\mathbf{a}_0\otimes\mathbf{a}_0 + \mathbf{a}_0\otimes\mathbf{a}_0\otimes\mathbf{I}\right)$$

$$+ \bar{\delta}_6 \left(\bar{\mathbf{C}}\otimes\mathbf{a}_0\otimes\mathbf{a}_0 + \mathbf{a}_0\otimes\mathbf{a}_0\otimes\bar{\mathbf{C}}\right) + \bar{\delta}_7 \left(\mathbf{a}_0\otimes\mathbf{a}_0\otimes\mathbf{a}_0\otimes\mathbf{a}_0\right)$$

$$+ \bar{\delta}_8 \left(\mathbf{I}\otimes\frac{\partial \bar{I}_5}{\partial\bar{\mathbf{C}}} + \frac{\partial \bar{I}_5}{\partial\bar{\mathbf{C}}}\otimes\mathbf{I}\right) + \bar{\delta}_9 \left(\bar{\mathbf{C}}\otimes\frac{\partial \bar{I}_5}{\partial\bar{\mathbf{C}}} + \frac{\partial \bar{I}_5}{\partial\bar{\mathbf{C}}}\otimes\bar{\mathbf{C}}\right) + \bar{\delta}_{10}\left(\frac{\partial \bar{I}_5}{\partial\bar{\mathbf{C}}}\otimes\frac{\partial \bar{I}_5}{\partial\bar{\mathbf{C}}}\right)$$

$$+ \bar{\delta}_{11}\left(\mathbf{a}_0\otimes\mathbf{a}_0\otimes\frac{\partial \bar{I}_5}{\partial\bar{\mathbf{C}}} + \frac{\partial \bar{I}_5}{\partial\bar{\mathbf{C}}}\otimes\mathbf{a}_0\otimes\mathbf{a}_0\right) + \bar{\delta}_{12}\frac{\partial^2 \bar{I}_5}{\partial\bar{\mathbf{C}}\partial\bar{\mathbf{C}}}\Big)$$

$$\tilde{\mathbb{P}} = \mathbf{C}^{-1}\odot\mathbf{C}^{-1} - \frac{1}{3}\mathbf{C}^{-1}\otimes\mathbf{C}^{-1}$$

$$\mathbb{C}_{\text{iso}} = \mathbb{P} : \bar{\mathbb{C}} : \mathbb{P}^{\top} + \frac{2}{3} J^{-2/3}\bar{\mathbf{S}} : \mathbf{C}\,\tilde{\mathbb{P}} - \frac{2}{3}\left(\mathbf{C}^{-1}\otimes\mathbf{S}_{\text{iso}} + \mathbf{S}_{\text{iso}}\otimes\mathbf{C}^{-1}\right)$$

Then, $\mathbb{C} = \mathbb{C}_{\text{vol}} + \mathbb{C}_{\text{iso}}$ can be calculated.

### 1.4.5 Nonlinear Solver for the Solid Mechanics Model

The governing nonlinear system of equations is solved by a Newton scheme. We define the vector of the unknown degrees of freedom as $(\hat{\mathbf{u}}, \hat{p}) =: \mathbf{z}$. Then, the nonlinear equation takes the general form $\mathbf{W}(\mathbf{z}) = 0$. By linearization around a value $\mathbf{z}$, we get

$$\mathbf{W}(\mathbf{z} + \Delta\mathbf{z}) = \mathbf{W}(\mathbf{z}) + \mathbf{J}\,\Delta\mathbf{z} + o(\mathbf{z} + \Delta\mathbf{z}),$$

with the increment $\Delta\mathbf{z} = (\Delta\hat{\mathbf{u}}, \Delta\hat{p})$ and the Jacobian matrix $\mathbf{J} = \partial\mathbf{W}/\partial\mathbf{z}$. Neglecting the sublinear error term $o(z + \Delta z)$, we can start from an initial guess $\mathbf{z}^{(0)}$ and proceed to find the root of $\mathbf{W}$ using the the following iterative Newton scheme:

$$\mathbf{J}\,\Delta\mathbf{z}^{(n)} = -\mathbf{W}(\mathbf{z}^{(n)}), \tag{1.81a}$$

$$\mathbf{z}^{(n+1)} = \mathbf{z}^{(n)} + \Delta\mathbf{z}^{(n)}. \tag{1.81b}$$

Equation (1.81a) is a linear system of equations with the system matrix given by $\mathbf{J}$, which has to be solved in every iteration step $n$. The linear system of equations can be expressed

as follows:

$$\begin{bmatrix} \mathbf{k}_{\delta\mathbf{u},\Delta\mathbf{u}} & \mathbf{k}_{\delta p,\Delta\mathbf{u}}^{\top} \\ \mathbf{k}_{\delta p,\Delta\mathbf{u}} & \mathbf{0} \end{bmatrix} \begin{bmatrix} \Delta\hat{\mathbf{u}} \\ \Delta\hat{p} \end{bmatrix} = \begin{bmatrix} -\mathbf{R}_{\delta\mathbf{u}} \\ -\mathbf{R}_{\delta p} \end{bmatrix}. \tag{1.82}$$

The definition of the right hand sides $\mathbf{R}_{\delta\mathbf{u}} = \delta W_{\text{int}} - \delta W_{\text{ext}}$ and $\mathbf{R}_{\delta p} = D_{\delta p}\Pi_L$ is given in Eq. (1.77). The system matrix is composed as follows. The upper left part consists of 3 times 3 blocks of submatrices, each with size $N_u \times N_u$ and the entries given by:

$$\mathbf{k}_{\delta\mathbf{u},\Delta\mathbf{u},(L,a),(M,b)} = \int_\Omega \phi^L_{(a),B} \tilde{k}_{abBD} \phi^M_{(b),D} \,\mathrm{d}V \quad \text{with} \quad \tilde{k}_{abBD} = \delta_{ab} S_{BD} + F_{aA} F_{bC} \mathbb{C}_{ABCD}.$$

Here, $S_{BD}$ and $\mathbb{C}_{ABCD}$ are entries of the second Piola-Kirchhoff stress tensor $\mathbf{S}$ and the elasticity tensor $\mathbb{C}$. The computation of these terms uses the description in Sec. 1.4.4.

The lower left part of the system matrix in Eq. (1.82) is given by 1 times 3 blocks of submatrices, each with size $N_p \times N_u$ and entries given by:

$$\mathbf{k}_{\delta p,\Delta\mathbf{u},L,(M,a)} = \int_\Omega J \, \psi^L \, (F^{-1})_{Ba} \, \phi^M_{(a),B} \,\mathrm{d}V.$$

The upper right part equals the transposed lower left block such that the system matrix is symmetric. Solving the system in Eq. (1.82) in every iteration of the Newton scheme in Eq. (1.81) converges to the solution of the static solid mechanics problem.

### 1.4.6 Discretization and Solution of the Dynamic Hyperelastic Model

The dynamic model is given by the system of nonlinear equations in Eq. (1.83). In addition to the spatial discretization with Finite Elements, we need to discretize the temporal derivatives of the displacement field $\mathbf{u}$ and the velocity field $\mathbf{v}$. The time derivatives are discretized to timesteps $t = i \cdot dt$ with an implicit Euler scheme:

$$\dot{\mathbf{u}} \rightsquigarrow \frac{1}{dt}(\mathbf{u}^{(i+1)} - \mathbf{u}^{(i)}), \qquad \dot{\mathbf{v}} \rightsquigarrow \frac{1}{dt}(\mathbf{v}^{(i+1)} - \mathbf{v}^{(i)}).$$

Because of the added inertial body force, the external virtual work now depends on the vector of unknowns. In consequence, we split the external virtual work $\delta W_{\text{ext}}$ into a

dead part $\delta W_{\text{ext,dead}}$ that solely depends on external forces and an inertial part:

$$\delta W_{\text{ext}} = \delta W_{\text{ext,dead}} + \int_\Omega \rho_0 \frac{v_{(a)}^{(i+1),L} - v_{(a)}^{(i),L}}{dt} \phi_{(a)}^L \phi_{(a)}^M \delta \hat{u}_a^M \, \mathrm{d}V = 0.$$

In summary, the system of equations to proceed from timestep $i$ to $(i+1)$ is given as:

$$\delta W_{\text{int}}(\mathbf{u}^{(i+1)}, p^{(i+1)}) - \delta W_{\text{ext}}(\mathbf{v}^{(i)}, \mathbf{v}^{(i+1)}) = 0 \qquad \forall\, \delta\mathbf{u}, \tag{1.83a}$$

$$\frac{1}{dt}(\mathbf{u}^{(i+1)} - \mathbf{u}^{(i)}) - \mathbf{v}^{(i+1)} = 0, \tag{1.83b}$$

$$D_{\delta p}\Pi_L(\mathbf{u}^{(i+1)}) = 0 \qquad \forall\, \delta p. \tag{1.83c}$$

Here, Eq. (1.83a) is the principle of virtual work, Eq. (1.83b) relates displacements $\mathbf{u}$ and velocities $\mathbf{v}$ and Eq. (1.83c) is the incompressibility constraint.

The system is again solved using the Newton scheme presented in Sec. 1.4.5. The linear system for each Newton iteration takes the following form:

$$\begin{bmatrix} \mathbf{k}_{\delta\mathbf{u},\Delta\mathbf{u}} & \mathbf{l}_{\delta\mathbf{u},\Delta\mathbf{v}} & \mathbf{k}_{\delta p,\Delta\mathbf{u}}^\top \\ \mathbf{l}_{\delta\mathbf{v},\Delta\mathbf{u}} & \mathbf{l}_{\delta\mathbf{v},\Delta\mathbf{v}} & \mathbf{0} \\ \mathbf{k}_{\delta p,\Delta\mathbf{u}} & \mathbf{0} & \mathbf{0} \end{bmatrix} \begin{bmatrix} \Delta\hat{\mathbf{u}} \\ \Delta\hat{\mathbf{v}} \\ \Delta\hat{p} \end{bmatrix} = \begin{bmatrix} -\mathbf{R}_{\delta\mathbf{u}} \\ -\mathbf{R}_{\delta\mathbf{v}} \\ -\mathbf{R}_{\delta p} \end{bmatrix}.$$

The entries $\mathbf{k}_{\delta\mathbf{u},\Delta\mathbf{u}}$ and $\mathbf{k}_{\delta p,\Delta\mathbf{u}}$ are the same as in the static case in Eq. (1.82). The other non-zero entries are given by

$$\mathbf{l}_{\delta\mathbf{u},\Delta\mathbf{v},(L,a),(M,b)} = \frac{1}{dt}\delta_{ab}\int_\Omega \rho_0 \, \phi_{(b)}^M \phi_{(a)}^L \, \mathrm{d}V, \qquad \mathbf{l}_{\delta\mathbf{v},\Delta\mathbf{u},(L,a),(M,b)} = \frac{1}{dt}\delta_{ab}\,\delta^{LM},$$

$$\mathbf{l}_{\delta\mathbf{v},\Delta\mathbf{v},(L,a),(M,b)} = -\delta_{ab}\,\delta^{LM}.$$

Note that in the dynamic problem, the system matrix is unsymmetric. It would be symmetric if the entries $\mathbf{l}_{\delta\mathbf{u},\Delta\mathbf{v}}$ and $\mathbf{l}_{\delta\mathbf{v},\Delta\mathbf{u}}^\top$ were be the same. This would be the case for a density of one, $\rho_0 = 1$, and if the term $\int_\Omega \phi_b^M \phi_a^L \, \mathrm{d}V$ would be replaced by $\delta_{ab}\delta^{LM}$. The second condition means that a lumped mass matrix would be used where the diagonal entries are set to the row sums of the original matrix.

We discretize the Finite Element solution in space by *Taylor-Hood* elements. This type of element uses quadratic ansatz functions $\phi$ for the displacements and velocities and

linear ansatz functions $\psi$ for the Lagrange multiplier or hydrostatic pressure $p$ on a 3D hexahedral mesh. This choice was proven to exhibit no locking [Zie05]. Locking is a phenomenon of degraded convergence of the Finite Element method for solid mechanics problems and occurs for improper discretization schemes.

For a compressible material, the incompressibility constraint which is the last equation in the systems Eq. (1.77) or Eq. (1.83) is removed. Instead of solving for the pressure $p$ as a Lagrange multiplier, the value is given by the constitutive model as described in Sec. 1.2.6. In consequence, the system matrix of the linear system of equations that is solved in the Newton iterations has a smaller size for compressible materials.

Moreover, the size varies depending on whether the static or the dynamic problem given in Sections 1.4.5 and 1.4.6 is solved. Assuming a linear mesh with $N_p$ degrees of freedom and a quadratic mesh with $N_u$ degrees of freedom, the square system matrix has $3N_u$ rows and columns for a static compressible formulation, $3N_u + N_p$ for a static incompressible formulation, $6N_u$ for a dynamic compressible model, and $6N_u + N_p$ for a dynamic incompressible model.

In any case, the mechanics model can be linked to the subcellular model by defining the active stress as given in Eq. (1.40). Since the active stress does not depend directly on the passive behavior, the active stress term can be added as a constant to the passive stress term. This constant also has no influence on the jacobian matrix $\mathbf{J}$. As the subcellular model depends on the fiber stretch $\lambda_f = \sqrt{I_4}$, there is a feedback loop between the subcellular and the solid mechanics model.

Details on the connection to the subcellular model as well as details on the numeric solution schemes for the nonlinear Newton solver and the linear solvers in every Newton iteration, including the solver schemes, how initial values are chosen and measures to speed up convergence such as load stepping are discussed in the implementation and result sections.

TODO

# Bibliography


[Car17] **Carniel**, T. A.; **Fancello**, E. A.: *A transversely isotropic coupled hyperelastic model for the mechanical behavior of tendons*, Journal of Biomechanics 54, 2017, pp. 49–57, ISSN: 0021-9290, doi:https://doi.org/10.1016/j.jbiomech.2017.01.042, https://www.sciencedirect.com/science/article/pii/S0021929017300726

[Cis08] **Cisi**, R. R.; **Kohn**, A. F.: *Simulation system of spinal cord motor nuclei and associated nerves and muscles, in a web-based architecture*, Journal of computational neuroscience 25.3, 2008, pp. 520–542

[Cra47] **Crank**, J.; **Nicolson**, P.: *A practical method for numerical evaluation of solutions of partial differential equations of the heat-conduction type*, Mathematical Proceedings of the Cambridge Philosophical Society 43.1, 1947, pp. 50–67, doi:10.1017/S0305004100023197

[Gui03] Godunov-type Schemes, ed. by **Guinot**, V., Amsterdam: Elsevier, 2003, pp. 471–480, isbn:978-0-444-51155-3, doi:https://doi.org/10.1016/B978-044451155-3/50015-3, https://www.sciencedirect.com/science/article/pii/B9780444511553500153

[Hei13] **Heidlauf**, T.; **Röhrle**, O.: *Modeling the chemoelectromechanical behavior of skeletal muscle using the parallel open-source software library opencmiss*, Computational and Mathematical Methods in Medicine 2013, 2013, pp. 1–14, doi:10.1155/2013/517287, http://dx.doi.org/10.1155/2013/517287

[Hei15] **Heidlauf**, T., ed.: *Chemo-electro-mechanical modelling of the neuromuscular system*, Englisch, Text (nur für elektronische Ressourcen), Online publiziert 2016, Stuttgart, 2015, http://nbn-resolving.de/urn:nbn:de:bsz:93-opus-104496

[Hin76] **Hinton**, E.; **Rock**, T.; **Zienkiewicz**, O. C.: *A note on mass lumping and related processes in the finite element method*, Earthquake Engineering & Structural Dynamics 4.3, 1976, pp. 245–249, doi:10.1002/eqe.4290040305

[Hod52a] **Hodgkin**, A. L.; **Huxley**, A. F.: *A quantitative description of membrane current and its application to conduction and excitation in nerve.* The Journal of Physiology 117.4, 1952, pp. 500–544

[Hod52b] **Hodgkin**, A. L.; **Huxley**, A. F.: *Propagation of electrical signals along giant nerve fibres*, Proceedings of the Royal Society of London. Series B, Biological Sciences, 1952, pp. 177–183

[Hol00] **Holzapfel**, A. G.: *Nonlinear solid mechanics*, 2000

[Klo20] **Klotz**, T. et al.: *Modelling the electrical activity of skeletal muscle tissue using a multi-domain approach*, Biomechanics and Modeling in Mechanobiology 19.1, 2020, pp. 335–349, ISSN: 1617-7940, doi:10.1007/s10237-019-01214-5, https://doi.org/10.1007/s10237-019-01214-5

[Mar94] **Marsden**, J. E.; **Hughes**, T. J.: *Mathematical foundations of elasticity*, Courier Corporation, 1994

[Mil06a] **Mileusnic**, M. P.; **Loeb**, G. E.: *Mathematical models of proprioceptors. ii. structure and function of the golgi tendon organ*, Journal of Neurophysiology 96.4, 2006, PMID: 16672300, pp. 1789–1802, doi:10.1152/jn.00869.2005, eprint: https://doi.org/10.1152/jn.00869.2005, https://doi.org/10.1152/jn.00869.2005

[Mil06b] **Mileusnic**, M. P. et al.: *Mathematical models of proprioceptors. i. control and transduction in the muscle spindle*, Journal of Neurophysiology 96.4, 2006, PMID: 16672301, pp. 1772–1788, doi:10.1152/jn.00868.2005, eprint: https://doi.org/10.1152/jn.00868.2005, https://doi.org/10.1152/jn.00868.2005

[Mor15] **Mordhorst**, M.; **Heidlauf**, T.; **Röhrle**, O.: *Predicting electromyographic signals under realistic conditions using a multiscale chemo-electro-mechanical finite element model*, Interface Focus 5.2, 2015, pp. 1–11, doi:10.1098/rsfs.2014.0076, http://dx.doi.org/10.1098/rsfs.2014.0076

[Pes79] **Peskoff**, A.: *Electric potential in three-dimensional electrically syncytial tissues*, Bulletin of mathematical biology 41.2, 1979, pp. 163–181

[Röh12] **Röhrle**, O.; **Davidson**, J. B.; **Pullan**, A. J.: *A physiologically based, multi-scale model of skeletal muscle structure and function*, Frontiers in Physiology 3, 2012

[Sho07] **Shorten**, P. R. et al.: *A mathematical model of fatigue in skeletal muscle force contraction*, Journal of Muscle Research and Cell Motility 28.6, 2007, pp. 293–313, doi:10.1007\%2Fs10974-007-9125-6, http://dx.doi.org/10.1007%5C%2Fs10974-007-9125-6

[Str68] **Strang**, G.: *On the construction and comparison of difference schemes*, SIAM Journal on Numerical Analysis 5.3, 1968, pp. 506–517, doi:10.1137/0705041, eprint: https://doi.org/10.1137/0705041, https://doi.org/10.1137/0705041

[Sus87] **Sussman**, T.; **Bathe**, K.-J.: *A finite element formulation for nonlinear incompressible elastic and inelastic analysis*, Computers & Structures 26.1, 1987, pp. 357–409, ISSN: 0045-7949, doi:https://doi.org/10.1016/0045-7949(87)90265-3, http://www.sciencedirect.com/science/article/pii/0045794987902653

[Tun78] **Tung**, L.: *A bi-domain model for describing ischemic myocardial dc potentials*. PhD thesis, Massachusetts Institute of Technology, 1978

[Zie05] **Zienkiewicz**, O. C.; **Taylor**, R. L.; **Zhu**, J. Z.: *The finite element method: its basis and fundamentals*, Elsevier, 2005

[Zie77] **Zienkiewicz**, O. C.; **Taylor**, R. L.: *The finite element method*, vol. 3, McGraw-hill London, 1977